

AMERICAN UNIVERSITY OF BEIRUT

THERMAL MODELING OF FUEL CELL HYBRID ELECTRIC
VEHICLES

by
LEILA MUNIR TABBARA

A thesis
submitted in partial fulfillment of the requirements
for the degree of Master of Engineering
to the Department of Electrical and Computer Engineering
of the Faculty of Engineering and Architecture
at the American University of Beirut

Beirut, Lebanon
April 2017

AMERICAN UNIVERSITY OF BEIRUT

THERMAL MODELING OF FUEL CELL HYBRID ELECTRIC
VEHICLE

by

LEILA MUNIR TABBARA


Approved by:

Dr. Sami Karaki, Chairperson
Electrical and Computer Engineering



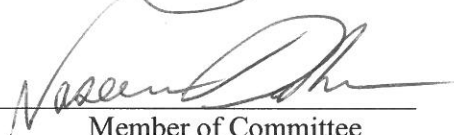
Advisor

Dr. Rabih Jabr, Professor
Electrical and Computer Engineering



Member of Committee

Dr. Naseem Daher, Assistant Professor
Electrical and Computer Engineering



Member of Committee

Date of thesis defense: April 26, 2017

AMERICAN UNIVERSITY OF BEIRUT

THESIS, DISSERTATION, PROJECT RELEASE FORM

Student Name: Tabbara Leila Munir
Last First Middle

Master's Thesis Dissertation Master's Project Doctoral

I authorize the American University of Beirut to: (a) reproduce hard or electronic copies of my thesis, dissertation, or project; (b) include such copies in the archives and digital repositories of the University; and (c) make freely available such copies to third parties for research or educational purposes.

I authorize the American University of Beirut, to: (a) reproduce hard or electronic copies of it; (b) include such copies in the archives and digital repositories of the University; and (c) make freely available such copies to third parties for research or educational purposes
after: **One --- year from the date of submission of my thesis, dissertation, or project.**
Two --- years from the date of submission of my thesis, dissertation, or project.
Three --- years from the date of submission of my thesis, dissertation, or project.

Leila Tabbara May 4 2017
Signature Date

ACKNOWLEDGMENTS

I would like to express my genuine appreciation to everyone who made this thesis possible. My up most gratitude to Prof. Sami Karaki for his supervision and guidance throughout my learning journey, and to the committee members, Prof. Naseem Daher and Prof. Rabih Jabr for their advice and support.

Thank you to all faculty members of the Electrical and Computer Engineering department, particularly Mrs. Rabab Abi Shakra for her help in the past couple of years. Big thanks to my friends for always being there for me and a special thanks to my family for their never-ending encouragement. Finally, thank you American University of Beirut for all the opportunities you have given me.

AN ABSTRACT OF THE THESIS OF

Leila Munir Tabbara for Master of Engineering
Major: Electrical and Computer Engineering

Title: Thermal modeling of fuel cell hybrid electric vehicles

The goal of this thesis is to model the behavior of a fuel cell hybrid electric vehicle (FCHEV) taking into consideration the effect of temperature on the overall vehicle performance. The fuel cell is intended to be the main energy provider in the vehicle. It receives humidified hydrogen from the tank and compressed air from the environment to deliver the required power. The battery on the other hand, is available to complement the existing fuel cell.

In addition to the above main components, the auxiliary systems consisting of a humidifier, a compressor and two cooling systems (one for the fuel cell and another for the battery), are designed. Water management in the fuel cell is critical; where low humidity causes the dryness of the membrane while excess humidity causes its flooding. So a humidifier is used to keep the membrane of the fuel cell at a good humidity level. A compressor receives the air intake from the atmosphere, and compresses it to reach the fuel cell operating pressure. Finally, the fuel cell and the battery are cooled separately since they have different operating temperatures.

The total power demand of the vehicle is derived from the specifications of the vehicle, the car speed and the road inclination angle. An energy management system is then combined to this model to distribute the power between the fuel cell and the battery pack with an aim to reduce the fuel consumption in the vehicle.

The overall model is then tested with three different car sizes. Each car runs through two different driving cycles (UDDS and HWFET) and with two battery modes (charge depletion (CD) and charge sustaining (CS)). Furthermore, the road inclination angle is increased and the car performance is observed when the car goes through the same runs as described above.

CONTENTS

ACKNOWLEDGMENTS.....	IV
ABSTRACT.....	V
LIST OF ILLUSTRATIONS.....	VI
LIST OF TABLES.....	VII
Chapter	
I.INTRODUCTION.....	1
A.Problem importance.....	1
B.Literature Review.....	1
C.ThesisContribution.....	7
II. Fuel cell model.....	8
A.Chapter overview.....	8
B.Introduction.....	8
C.Fuel cell theory of operation.....	9
D.Electrical model.....	11
E.Thermal model.....	15
F.Results.....	20
III. Battery model.....	22
A.Chapter overview.....	22
B.Introduction.....	22
C.Lithium ion Battery theory of operation.....	23

D.Electrical model.....	25
E.Thermal model.....	32
F.Results.....	33
IV. Auxiliaries and hydrogen tank.....	36
A.Chapter overview.....	36
B.Cooling system.....	36
C.Humidifier.....	40
D.Compressor model.....	43
E.Hydrogen tank model.....	43
V- System integration.....	46
A.Model integration.....	46
B.Energy management system.....	50
VI- Model validation and test results	53
A.Introduction.....	54
B.Speed profile.....	54
C.Car sizes.....	54
D.Model validation.....	57
E.Results.....	69
F.40 mile vehicle detailed results.....	73
VII- Conclusion.....	88
VIII-References.....	90

LIST OF ILLUSTRATIONS

Figures	Page
2.1 Construction of a PEMFC	11
2.2 Electric circuit of a fuel cell.....	15
2.3 Heat distribution in a fuel cell.....	16
2.4(a): Fuel cell polarization curve.....	21
2.4 (b): Power density curve.....	21
2.6 & 2.7: Fuel cell losses.....	21
3.1 Construction of a Li-ion Battery.....	24
3.2 Electrical circuit Model.....	25
3.3 Example of a battery voltage during a discharging resting interval.....	27
3.4 Open circuit voltage with respect to SOC.....	34
3.5 Series resistance.....	34
3.7& 3.8 long and short transient capacitance	35
4.1 The radiator	37
4.2 Cooling system components.....	38
4.3 Hydrogen tank schematic.....	45
5.2 Single FC assembly	47
5.1 Components integration in the vehicle.....	46
5.3 FC stack.....	47
5.4 FC –cooling system.....	48
5.5, 5.6 & 5.7 Battery cells.....	48

5.8 Battery module.....	49
5.9 Cooling channels in the battery module.....	49
5.10 Battery required power vs. SOC.....	53
6.1 Speed profile for an urban road (UDDS).....	54
6.2 Speed profile for a highway road (HWFET).....	54
6.3(a) Rule base power demand.....	56
6.3(b) DP power demand.....	56
6.4(a) Fuel cell and battery remaining energy in Rule base.....	57
6.4(b) Fuel cell and battery remaining energy in DP.....	63
6.5(a) Rule base power demand.....	65
6.5(b) DP power demand.....	65
6.6(a) Fuel cell and battery remaining energy in Rule base.....	62
6.6(b) Fuel cell and battery remaining energy in DP.....	63
6.7(a) Rule base power demand.....	64
6.7(b) DP power demand.....	64
6.8(a) Fuel cell and battery remaining energy in Rule base.....	65
6.8(b) Fuel cell and battery remaining energy in DP.....	66
6.9(a) Rule base power demand.....	67
6.9(b) DP power demand.....	67
6.10(a) Fuel cell and battery remaining energy in Rule base.....	70
6.10(b) fuel cell and battery remaining energy in DP.....	68
6.11 fuel cell and battery Power supplied.....	74
6.12 fuel cell (a) and battery (b) energy remaining.....	75

6.13 Auxiliary power.....	76
6.14 Heat rates in Fuel cell (a) and battery (b).....	78
6.15 Fuel cell (a) and battery (b) Temperatures.....	79
6.16 Pressure (a) and temperature (b) variation in hydrogen tank.....	84
6.17 fuel cell and battery Power supplied.....	85
6.18 fuel cell (a) and battery (b) energy remaining.....	86
6.19 Auxiliary power.....	83
6.20 Heat rates in Fuel cell (a) and battery (b).....	85
6.21 Fuel cell (a) and battery (b) Temperatures.....	86
6.22 Pressure (a) and temperature (b) variation in hydrogen tank.....	87

LIST OF TABLES

Table	Page
2.1 Different Types of FCs.....	9
2.2 Gibbs free energy at different temperatures	12
2.3 Parameters used in validation.....	20
3.1 Different types of batteries	23
3.2 Discharging Parameters	28
3.3 Charging Parameters	29
3.4 OCV Parameters	29
3.5 Impedance Parameters for charging	31
3.6 Impedance Parameters for Discharging	31
4.1 Specifications of the Cooling System Components	38
4.2 Saturated Vapor Pressure of Water at Different Temperatures	42
6.1 Fuel cell and Battery Specifications.....	55
6.2 Car Specifications	55
6.3 Car Mass Distribution	56
6.4 Rule Base versus DP—Charge Depletion Mode.....	57
6.5 Rule Base versus DP—Charge Depletion Mode-HWFET.....	64
6.6 Rule Base versus DP—Charge Sustaining Mode-UDDS.....	63
6.7 Rule Base versus DP—Charge Sustaining Mode-HWFET.....	66
6.8 Car1 Operation at UDDS.....	74
6.9 Car1 Operation at HWFET.....	70

6.11 Car2 Operation at HWFET.....	75
6.12 All- Battery Car Operation at UDDS.....	72
6.13 All- Battery Car Operation at HWFET.....	73

CHAPTER 1

INTRODUCTION

A. Problem importance

The environmental impact of the transportation sector is enormous because it is a major user of energy. This creates air pollution, greenhouse gas emissions that enhance global warming, and health problems. Therefore, it is important to find a substitute that will decrease the harmful emissions of fossil fuels. Hydrogen is considered to be one of the best alternatives for fossil fuels due to its low polluting properties if it were produced from clean and sustainable energy. PEMFCs use hydrogen and are suitable for automotive applications because of their simplicity in construction, high efficiency and low operating temperatures.

To fulfill the requirements in automotive applications, a fuel cell must be coupled with a battery. The battery will help the fuel cell stack when needed and will capture the excess energy during regenerative braking and hence improve the total efficiency of the vehicle. Li-ion battery is the most used in electric vehicles [9]. However, traditional li-ion batteries have a short lifespan; so more variations on lithium ion batteries are being done that sacrifice the high energy density for a longer life span (e.g. Lithium iron phosphate).

B. Literature Review

1. Fuel cell

The fuel cell principle was discovered in 1839; but due to its high cost, this technology was not developed and used until 1960 (in the American Gemini space mission). Fuel cells came to the front in 1990 and were found to be applicable for stationary

and portable applications since they have a high power density [1]. When compared with ICE, they are more efficient, less polluting, have a quiet operation and less moving parts which made them suitable for automotive applications.

Damen [2] classified fuel cells according to their electrolyte membranes and their operating temperatures. Those operating at low temperatures are the alkaline fuel cell (AFC), phosphoric acid fuel cell (PAFC), and proton exchange membrane fuel cell (PEMFC). Others that operate at high temperatures are Molten Carbonate fuel cell (MCFC) and solid oxide fuel cell (SOFC). Larminie [3] mentioned that the PEMFC has been flourishing and developments in terms of power density improvements and cost reduction were brought to it since 1970. Its current density has increased to reach 1 A cm^{-2} , in addition to the reduction of platinum, which leads to the significant reduction in its cost per kW of power. FCs vary in several ways such as the method of cooling, their arrangement, and the reactants used. The two chemicals engaged in the reaction do not have to be hydrogen and oxygen. Yet since oxygen is available in air and hydrogen has a fast reaction kinetics, they are mostly used.

Temperature affects the operation of a fuel cell as it reflects on its reaction kinetics, flow of water, conductivity of the membrane, and the catalyst. Nevertheless, it was found that the optimum operating temperature of a fuel cell is at 80°C [4]. Larminie[3] differentiated between the methods used to dissipate heat in the cell, where temperature control is carried out using the cooling effect of the “cathode air supply” for low power PEMFCs (up to 100 W). On the other hand, fuel cells with higher power ratings (100W up to 1000W) are cooled using “separate air cooling” channels made in the bipolar plate. As for power ratings

higher than 1kW, air becomes inefficient and must be replaced by “liquid cooling.”

San Martin et al [5] were able to predict the voltage and operating temperatures of a 1.2 kW FC using an electrical and a thermal model. The proposed models were based on the integration of the thermodynamic and FC losses with a thermal model which is based on the thermal energy balance. The results were then validated at steady state and dynamic operating environments. The predicted outcomes had a 0.6V error as compared to the actual FC voltage and a 1.5 °C error in the predicted temperature of the fuel cell.

Shahsavari et al [6] developed a three dimensional thermal model to predict the temperature distribution in the PEM fuel cell. The proposed design can be used for modeling and optimization of various cooling devices. This model was used to simulate the 3D temperature profiles and estimate the maximum temperature in an air cooling system. It was then validated by comparing the results with experimental data.

Rojas et al [7] presented a thermal modelling approach of a water cooled PEM fuel cell. The model was based on a heat flux inside the stack. A linear model predictive control (MPC) strategy for temperature regulation of the output water was then adopted and tested.

2. Battery

Tremblay [8] chose the SOC to be the only state variable in his model which consists of a resistor put in series with a controlled voltage source. He then explains how to extract the circuit parameters from the manufacturer’s data sheet. The final model is then simulated and a discharge curve is obtained and validated with the manufacturer’s information.

Hongwen et al [9] proposed the dual polarization (DP) model where an RC circuit was added to the Partnership for a New Generation of Vehicles (PNGV) model, which takes into account the variation on the open circuit voltage in the time accumulation of the load current. The parameters of this model were found using a genetic algorithm. The dynamic performance test along with SOC estimation were conducted for this model and compared with traditional ones. It was found that the DP model has the best dynamic performance and a most accurate SOC.

Zeitouny et al [10] used a least squares estimation method in three different circuits, a single Randles cell, a double Randles cell, and a circuit using a finite Warburg impedance element. A set of experiments based on electro-impedance spectrometry (EIS) were done to obtain the internal battery parameters on a 12V, 4800 mAh Li-ion battery as well as on a 12 V, 7.2 Ah lead-acid battery. It was concluded that for a Li-ion battery the double Randles cell gave the best results at a frequency range between 1Hz and 1 kHz. On the other hand, at a frequency range between 0.1 Hz and 1 Hz the finite Warburg impedance element gave the best results for Lead-acid battery.

Same as a fuel cell, temperature affects the operation and health of the li-ion battery. It was observed that increasing the temperature increases the degradation rate of all the elements inside the battery, which include the maximum storage charge capacity, the effectiveness of the electrodes, and charge transfer rate [11].

The National Renewable Energy Laboratory (NREL) performed tests on lithium ion cells which showed that the cell responds very well at temperatures from around 22°C to

50°C when the state of charge varies from 50% to 80% [12].

The modeling of battery cooling system would be similar to that of the fuel cell but will have to be separate since the operating temperature of the battery is in the range 35 to 40°C.

Pesaran [13] discussed different cooling systems for batteries used in hybrid electric vehicles. He started by passive cooling using ambient air, which is considered to be sufficient to cool the battery pack in mild climates. For more extreme climates, an active cooling system is needed to cool the battery pack. This could be achieved by blowing air across the modules or by liquid cooling. Liquid cooling is more effective than air cooling and takes up less volume, but it could have higher mass, leakage issues, and require more maintenance.

3. Fuel cell car models

Rizzoni et al [14] presented a methodology that permits easy and fast energy analysis using quasi-static simulations. This approach starts from a given speed profile and uses the road load to calculate the acceleration, velocity and distance backwards (from the wheel to the tank). This permits the total estimation of fuel and electric energy consumption. After the comparison between the conventional and parallel hybrid Sport Utility Vehicle, it was found that the proposed design is applicable.

Bernard et al [15] suggested a real time control strategy that is derived from an optimum control algorithm. The experiments done were based on a 600W FC system and a

lead acid battery, and showed reduction in the fuel consumption with both experimental results and simulation results. The experiments were conducted at controlled and constant temperatures.

Karaki et al [16] used an energy management system for fuel cell hybrid electric vehicles to minimize the use of hydrogen as well as the battery degradation. Using forward dynamic programming, a set of constraints were defined including the power balance at each stage, power limits, state-of-charge limits, and ramp rate constraints. This method gave fast results with UDDS and HWFET standard driving cycles. Karaki et al [17] designed a fuel cell hybrid vehicle using ordinal optimization (OO) and dynamic programming (DP) with an aim to reduce hydrogen fuel consumption, operating and total investment cost. Under specific driving cycles and vehicle components, the DP provides the total cost per year. OO then produces a set of “good enough” designs and sorts them in an ascending order where the best designs are then selected and evaluated. Different tests were performed on the selected top designs with different sizes of fuel cells, batteries, and hydrogen tanks. Majed et al [18] described a single step dynamic programming (SSDP) for FCHEV, which was used to decrease the cost of hydrogen and battery degradation taking into account the charge sustaining (CS) and charge depleting (CD) strategies of the battery. Same as the DP method, SSDP uses power balance, the fuel cell and battery power limits, battery state-of-charge limits, and the ramp rates as constraints of the fuel cell and battery. It works on a one step ahead speed forecast instead of the entire driving cycle, which makes it much faster than DP and possible for real-time implementation. It is worth mentioning that the results of fuel economy and system cost for both methods are close to each other.

C. Thesis Contribution

The objective of this thesis is to understand how temperature affects the behavior of the fuel cell and the battery present in FCHEVs. This can be achieved through the development of electrical models for the fuel cell and the battery that is dependent on temperature. A thermal model is also established that represents the heat variation inside the fuel cell and the battery. Furthermore, a cooling system is proposed to keep the temperature of the above components at the required operating level. Dynamic energy balance equations were used to determine the temperature based on estimation of the thermal mass of the system, heat generated inside the system, heat lost by cooling, radiation and convection. After that, the power demand of each component in the model is obtained using a rule base energy management system. Where it differentiates between three operating modes of the vehicle, the motoring mode, the generating mode and the idling mode. The auxiliaries in the system including the humidifier and the compressor were also modeled to control the humidity level in the fuel cell and to maintain a pressurized air at the anode.

This work adds precision to the FC hybrid electric vehicle model, where the temperature effect on each component is being taken into consideration. The temperature affects the power consumed by the auxiliaries and the power supplied by the FC and the battery. This can be clearly monitored in this design. In addition to that, external factors affecting the FCHEV operation can be easily modified for its testing, such as the ambient temperature and the road inclination angle.

Chapter2

Fuel cell model

A. Chapter overview

An electrical circuit model is used to describe the behavior of the fuel cell. Where the output voltage of the fuel cell is obtained from the open circuit voltage, the activation losses, concentration losses, and ohmic losses. In addition to that, a thermal modeling for the fuel cell is represented which takes into consideration the heat generated, the heat lost to the environment, and the heat lost to the cooling system.

B. Introduction

Fuel cells are energy conversion devices which convert chemical energy into electrical energy. It is where hydrogen and oxygen are combined to produce an electric current.

Several types of fuel cells are available each having a suitable application.

1. Proton Exchange Membrane fuel cell (PEMFC)
2. Alkaline Electrolyte fuel cell (AFC)
3. Direct Methanol fuel cell (DMFC)
4. Phosphoric Acid fuel cell (PAFC)
5. Molten Carbonate fuel cell (MCFC)
6. Solid Oxide fuel cell (SOFC)

From table 2.1, it is shown that PEMFCs are the most suitable in vehicle applications. This is due to its low operating temperature, high efficiency, and high power output. In addition to its fast startup time (<30 sec.), its low noise operation, and ultra-low pollution [19].

Table 2.1 Different Types of FCs

	AFC	MCFC	PAFC	SOFC	PEMFC
Electrolyte	Potassium hydroxide	Immobilized liquid molten carbonate	Immobilized liquid phosphoric acid	Ceramic	Ion exchange membrane
Operating Temperature	60°C – 90°C	650°C	200°C	1000°C	80°C
Efficiency	45 – 60%	45 – 60%	35 – 40%	50 – 65%	40 – 60%
Electrical Power	Up to 20kW	>1MW	>50kW	>200kW	Up to 250kW
Possible applications	Submarines spaceships	Power stations	Power stations	Power stations	Vehicles

C. Fuel cell theory of operation

Oxidation of hydrogen takes place in a proton exchange membrane producing electricity, water and heat during the process. When hydrogen and oxygen are introduced into the FC, electrons flow from the anode to the cathode through the load circuit. On the other hand, H⁺ ions pass through the electrolyte to combine again with oxygen [3].

Equations below show the anode, the cathode and the full cell reactions.



The proton exchange membrane consists of a gas diffusion layer, a catalyst layer and an electrolyte as it is shown in Figure 2.1 [20]. Each of these layers have a purpose. The gas diffusion layer for instance has a good conductivity level, which helps in the movement of the reactants and the products. The membrane is the central layer. It allows the proton's transport from the anode to the cathode while preventing the crossing of electrons and gas. The catalyst layer separates the diffusion layer and the membrane and it is where the half equations (2.1 and 2.2) take place. The membrane should be hydrated to facilitate the movement of protons, yet extra hydration may cause the flooding of the membrane. This is why an effective water management is necessary

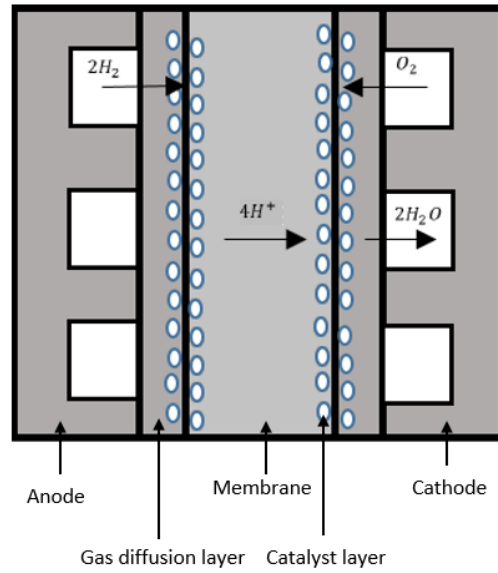


Figure 2.1 Construction of a PEMFC [20]

A PEM fuel cell can theoretically generate a 1.23V at standard temperature and pressure. For high voltage applications, several fuel cells are connected in series forming a stack. The anode of one cell and the cathode of the other are connected in series via a bipolar plate.

D. Electrical model

1. Nernst equation

Nernst Equation (2.4) represents the OC voltage (E_0) of a fuel cell. It consists of the open circuit voltage (E_{0c}) at standard temperature and pressure, in addition to another term that takes into consideration the effect of temperature and pressure variations.

$$E_0 = E_{0c} + \frac{RT}{2F} \ln \left(\frac{P_{H_2} P_{O_2}^{\frac{1}{2}}}{P_{H_2O}} \right) \quad (2.4)$$

P_{H_2}, P_{O_2} and P_{H_2O} are the partial pressures of hydrogen, oxygen and water respectively. T is the temperature, R is the ideal gas constant and F is faradays constant.

In a fuel cell, (E_{0c}) is related to the ‘‘Gibbs free energy’’ which symbolizes the movement of electrons in the circuit. Equation 2.5 consists of the number of the electrons (Z) transferred in a reaction for each molecule, Faraday’s constant, and the Gibbs energy(G_f) whose value is changing depending on temperature and the state of water.

$$E_{0c} = \frac{-G_f}{ZF} \quad (2.5)$$

Table 2.2 Gibbs free energy at different temperatures [3]

Form of water product	Temperature (°C)	Gf (KJ/mol)
Liquid	25	-237.2
Liquid	80	-228.2
Gas	80	-226.1
Gas	100	-225.2
Gas	200	-220.4
Gas	400	-210.3
Gas	600	-199.6
Gas	800	-188.6
Gas	1000	-177.4

2. *Activation losses*

Activation losses are the losses caused by the slowness of the reaction taking place at the surface of the electrode. These represent the amount of voltage lost in the transport of electrons to and from the electrodes.

Tafel observed in 1905 as a result of his experiments that the overvoltage at the surface of the electrodes follows a certain pattern in a variety of electrochemical reactions.

Tafel's equation can be expressed in many different forms. One of the best equations uses natural logarithmic as it is shown in the equation below:

$$\Delta V_{act} = A \ln \frac{i}{i_0} \quad (2.6)$$

Where i_0 is the “exchange current density” or the minimum current density at which the over voltage begins to move from zero. For this equation to hold, i must be greater than i_0 . Due to higher anode exchange current density, cathode activation losses are significantly higher so anode activation losses are negligible.

The constant “ A ” was deduced by McDougall in 1976 from the fact that two electrons per mole are transferred in a hydrogen fuel cell. It is represented as follows:

$$A = \frac{RT}{2\alpha F}$$

The constant α is called the “charge transfer coefficient”. Its value depends on the reaction involved and the material the electrode is made from. For the hydrogen electrode, its value is about 0.5 for a great variety of electrode materials (Davies, 1967). At the

oxygen electrode the charge transfer coefficient shows more variation, but is still between 0.1 and 0.5 in most circumstances [3].

3. Mass Transport or concentration losses

Concentration losses are due to the change in the concentration of the reactants at the surface of the electrodes. If air is supplied to the cathode side, there will be a slight pressure drop in oxygen at the level of the electrode. Similarly, at the anode, if pure hydrogen is being supplied, a pressure drop will occur. These pressure drops or concentration losses are a result of the amount of current being extracted from the cell, and hence will cause the voltage reduction. This can be represented as follows:

$$\Delta V_{trans} = -B \ln \left(1 - \frac{i}{i_L} \right) \quad (2.7)$$

B is different for the two reactants. It is $\frac{RT}{2F}$ for hydrogen, and $\frac{RT}{4F}$ for oxygen. And i_L is the current limiting, or the maximum current extracted from the fuel cell per unit area.

4. Ohmic Losses

Ohmic losses are the straight forward losses due to the internal resistance of the electrodes and the resistance to the flow of ions in the electrolyte. The voltage drop is given by:

$$\Delta V_{ohm} = ir \quad (2.8)$$

Where “ r ” is the area-specific resistance in $\Omega \text{ cm}^2$ and is mainly due to the membrane resistivity (ρ_m) and the thickness of the membrane (l).

$$r = \rho_m l$$

ρ_m is given as follows:

$$\rho_m = \frac{181.6 \left(1 + 0.03i + 0.062 \left(\frac{T}{300} \right) i^{2.5} \right)}{(\lambda - 0.634 - 3i) \exp(4.18 \left(\frac{T - 303}{T} \right))}$$

Where i is the current density, λ is the number of water molecules with respect to SO₃ molecules in the membrane, it is function of the relative humidity (ϕ_m)[21]:

$$\lambda = 0.043 + 17.81\phi_m - 39.85\phi_m^2 + 36\phi_m^3$$

5. Total cell Voltage

The output voltage (V_{out}) is derived from the electric circuit of the fuel cell (Figure 2.2) after subtracting the potentials associated with the activation losses (V_{act}), the ohmic losses (V_{ohm}), and the transport losses (V_{trans}) from the OC voltage (E_0).

$$V_{out} = E_0 - V_{act} - V_{ohm} - V_{tran}$$

(2.9)

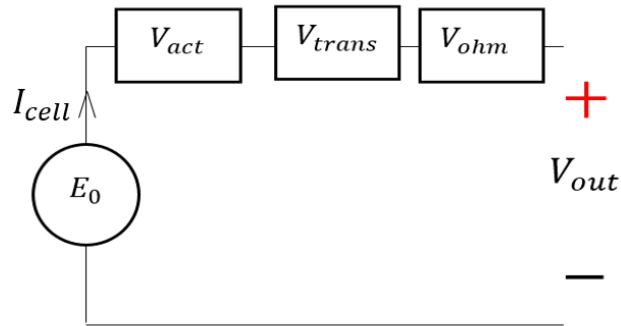


Figure 2.2 Electric circuit of a fuel cell

The power generated by the fuel cell stack is a product of the individual cell voltage, current and the number of cells (N). The current and voltage are related according to the polarization curve which is determined using the model. However for any given

power output a high fuel cell operating voltage leads to larger stack. Fuel cells are hence connected in series and parallel to reach the desired output power.

$$P = N \times V_{out} \times I_{cell} \quad (2.10)$$

E. Thermal model

Thermal energy is exchanged between physical systems to dissipate heat. This is done via three fundamental modes which are conduction, convection, and radiation. Conduction heat transfer is at a microscopic scale. When particles get heated they gain kinetic energy and transfer their heat to areas with lower kinetic energy. Convection happens when the air gets heated and travels away from the source it then carries the thermal energy along with it. Radiation on the other hand is due to the electromagnetic waves emitted. These waves carry the thermal energy away. In our thermal analysis, conduction is not taken into consideration since the thermal distribution of heat inside the fuel cell is assumed to be the same and the generated is equally distributed in the FC and the battery.

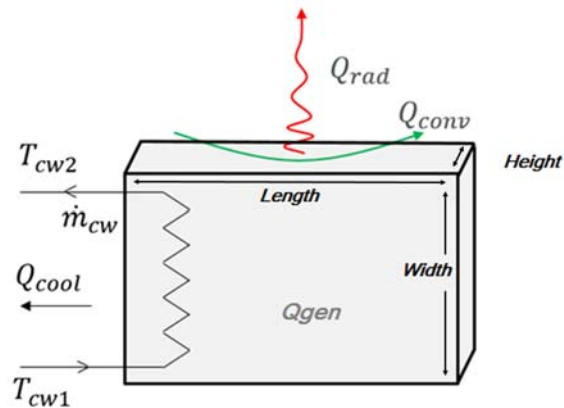


Figure 2.3 Heat distribution in a fuel cell

1. *Heat Generated*

A fuel cell is generating an amount of heat equal to the amount of power not consumed by the fuel cell [13]. So from the fuel cell efficiency (η_c) the heat generated can be calculated using the following equation:

$$Q_g = Num \left(\frac{1}{\eta_c} - 1 \right) \quad (2.11)$$

Where the fuel cell efficiency (η_c) is defined as the ratio between the output voltage (V_{out}) and the open circuit voltage (E_0) of the cell.

$$\eta_c = \frac{V_{out}}{E_0} \quad (2.12)$$

2. *Heat loss to environment*

As discussed earlier, the fuel cell loses heat to the environment via convection and radiation. First we calculate the area of the fuel cell stack rested on the ground which is represented as " A_b ".

$$A_b = 2 L W N_p + L H N + 2 W H N$$

N_p is the number of parallel strings in the stack, N is the total number of fuel cells in the stack in series and in parallel, L , W , H are the length, width and height of one single cell .

(a) Radiation:

To find the amount of heat loss due to radiation " Q_r " the equation below is used.

$$Q_r = \sigma \varepsilon A_b (T_c^4 - T_a^4) \quad (2.13)$$

Where σ the Stephan-Boltzmann is constant, ε is the emissivity of the fuel cell, T_a is the ambient temperature, and T_c is the fuel cell temperature.

(b) Convection

Two different types of convection happens inside the vehicle, where the amount of heat lost to convection is not the same if the car is moving or standing still. Natural convection takes place when the car is not moving, while forced convection happens when the car has a certain speed so the wind speed must be considered. The fuel cell stack is a rectangular block with horizontal and vertical surfaces.

To find the natural convection [22] in vertical surfaces, Nu is calculated as in equation 2.15.

Whereas for horizontal surfaces Nu is given as in equation 2.16.

$$Ra = \frac{g\beta(T_c - T_a)L_c^3}{\gamma\alpha} \quad (2.14)$$

$$Nu = 0.68 + \frac{0.67Ra^{\frac{1}{4}}}{\left(1 + \left(\frac{0.492}{Pr}\right)^{\frac{9}{16}}\right)^{\frac{4}{9}}} \quad (2.15)$$

$$Nu = 0.96 R^{\frac{1}{6}} \quad (2.16)$$

As for the forced convection [22], a cross flow and a parallel flow across the fuel cell is taking place. First Reynold number (Re) is calculated as:

$$Re = \frac{\rho V L_c}{\mu} \quad (2.17)$$

For the cross flow we calculate Nu as in the shown equations:

$$Nu = 0.177Re^{0.699}Pr^{1/3} \quad 2500 < Re < 8000 \quad (2.18)$$

$$Nu = 0.102Re^{0.675}Pr^{1/3} \quad 5000 < Re < 100,000 \quad (2.19)$$

For the parallel flow we calculate Nu as in the shown equations:

$$Nu = 0.664Re^{1/2}Pr^{1/3} \quad Re < 5 \times 10^5 \quad (2.20)$$

$$Nu = (0.037Re^{4/5} - 871)Pr^{1/3} \quad 5 \times 10^5 < Re < 10^8 \quad (2.21)$$

$$Nu = 0.037Re^{4/5}Pr^{1/3} \quad Re > 10^8 \quad (2.22)$$

For each surface in the fuel cell stack, the heat lost via convection (Q_{con}) is simply calculated as:

$$Q_{con} = h_c A_s (T_c - T_a) \quad (2.23)$$

Where the convective heat transfer coefficient $h_c = \frac{Nu k}{Lc}$

Ra is Rayleigh number, g is the gravitational constant β is the coefficient of volumetric expansion, ν is the kinematic viscosity, α is the thermal diffusivity of the fluid, ρ is the density of air, μ is the absolute viscosity, k is the thermal conductivity of air, Nu is the Nusselt number, Pr is Prandtl number Lc is the characteristic length which is equal to the total area of the cell divided by its perimeter, and V is the wind speed.

3. *Heat loss to the coolant*

The cooling system also contributes to the heat loss and is modeled as follows:

$$Q_{cc} = \dot{m}_c c_{lc} (T_{1c} - T_{2c}) \quad (2.24)$$

Where the heat lost to the coolant is (Q_{cc}), c_{lc} is the specific heat of the cooling liquid, T_{1c} and T_{2c} are the inlet and the outlet temperatures of the cooling liquid, and \dot{m}_c is the mass flow rate of the cooling liquid inside the fuel cell.

4. *Temperature of the cell*

The final heat rise is obtained by removing the heat loss from the generated heat:

$$Q_c = Q_g - Q_r - Q_{con} - Q_{cc} \quad (2.25)$$

Then the temperature variation in the cell is found from:

$$m_t C_t \frac{dT_{cell}}{dt} = Q_c \quad (2.26)$$

F. Results

The polarization curve shows how the voltage varies with current density. The polarization curve (Figure 2.4(a)) is obtained after removing the losses in the circuit which are the activation losses (Figure 2.5), transportation losses (Figure 2.6), and the ohmic losses (Figure 2.7). Each of the three over potentials have a different effect on the output voltage over the current range. The below curves were plotted for the fuel cell having the specification as in table 2.3. The activation losses dominates the low current density region, while the transportation losses affects the high current density region.

High temperatures increase the conductivity of the membrane so the chemical reaction becomes faster which increases the water production at the cathode and hydrates the membrane thus decrease the resistivity of the membrane [23]. This can be clearly seen in the Figures below where the output voltage increases at higher temperatures with the decrease in the ohmic losses.

The exchange current density	i_0	$2.8 \times 10^{-7} \text{ A cm}^{-2}$
The current limiting	i_L	0.9 A cm^{-2}
Width of the membrane	l	0.012 cm
Active area of the cell	A_{cell}	300 cm^2
Relative humidity equation	λ	10
Charge transfer coefficient	α	0.5

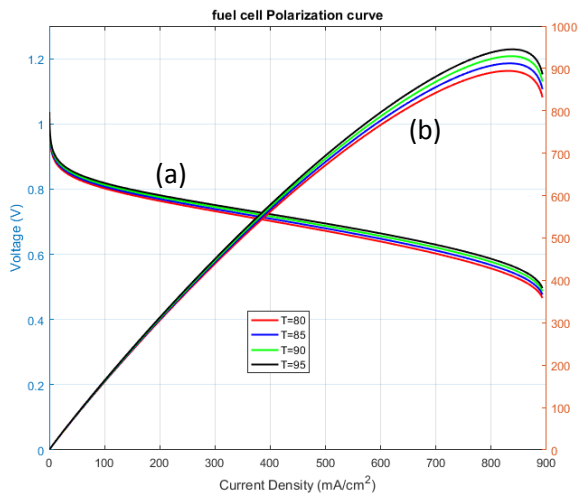


Figure 2.4(a): Fuel cell polarization curve losses

Figure 2.4 (b): Power density curve

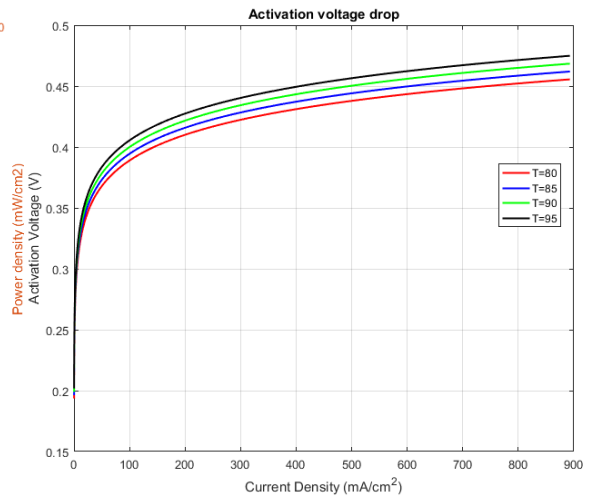


Figure 2.5: Fuel cell activation

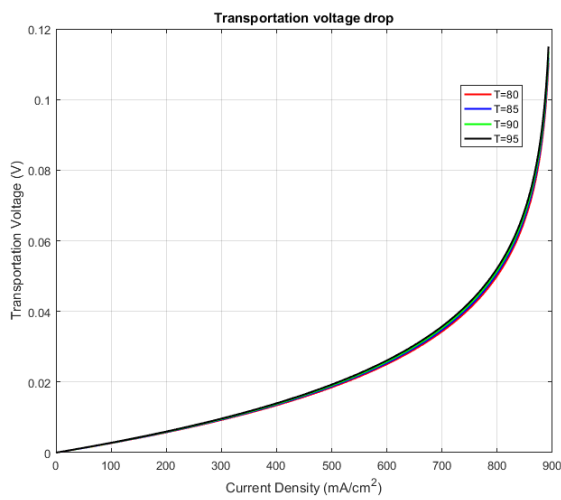


Figure 2.6: Fuel cell transportation losses

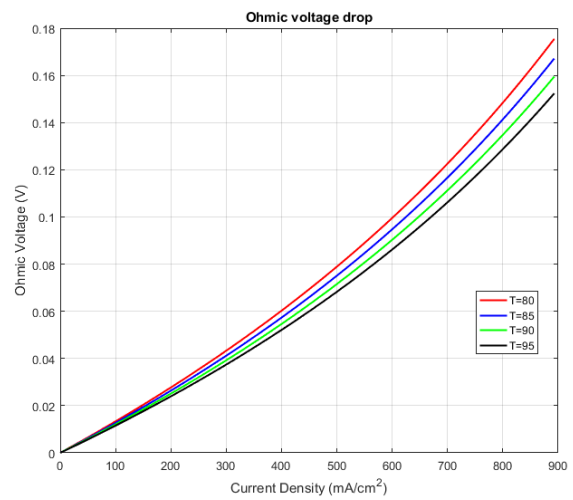


Figure 2.7: Fuel cell

CHAPTER3

BATTERY MODEL

A. Chapter overview

An electric circuit model of the battery is discussed along with the open circuit voltage and circuit impedances which depend on the state of charge and temperature. The equations used for the circuit components are from a previous work done by Long Lam [25]. Same as in chapter 2, a thermal model is also presented taking into account the heat generated and the heat lost to the cooling system.

B. Introduction

Lithium ion batteries are being widely used today to supply and store energy in electric vehicles. They have a low self-discharge, a high cycle life and high power and energy densities, which make them suitable for automotive applications. Several types of lithium ion batteries are available with varying pros and cons. For example, Lithium iron phosphate ($LiFePO_4$) will not experience a “thermal runaway”; which means that the increase in the cell temperature will not cause more heat that ceases their operation. In addition to the above advantage, they have the lowest cost per Ah and kW, a good life span, and are extremely safe [24]. Table (3.1) below compares different aspects in batteries that prove lithium ion batteries are in fact illegible for high power applications.

Table 3.1 Different types of batteries [25]

	Lead Acid	NiMH	Li-ion
Nominal cell voltage	2V	1.2V	2.5V/3.3V/3.6-3.7V
Specific energy	30-45 Wh/kg	30-80 Wh/kg	90-220 Wh/kg
Energy density	60-75 Wh/L	140-300 Wh/L	380-400 Wh/L
Specific power	180 W/kg	250-1000 W/kg	600-3400 W/kg
Cycle life	500-800	500-1000	1000-8000
Self-discharge	2 – 4%/month	20 – 30%/month	2 – 5%/month
Temperature range	–20 → 60°C	–20 → 60°C	–20 → 60°C
Relative costs	Low	Moderate	High

C. Lithium ion Battery theory of operation

Starting with some terms that describe the state and properties of battery cells [25]:

The state of health (SOH) is an indicator of the condition of the battery compared with its ideal state (fresh battery). So a SOH of 100% means that the battery functions perfectly as in the specifications.

The state of charge (SOC) is an indicator for the amount of charge in Ah left in the battery (the state of the useable capacity in the cell). Every model element in the battery circuit will therefore be dependent on the SOC. The SOC of the battery can be simply calculated from the initial SOC (SOC_0), the current (i) and the charging capacity of the battery (Q) as:

$$SOC(t) = SOC_0 - \frac{1}{Q} \int_0^t i(t) dt \quad (3.1)$$

The depth of discharge (DOD) is the inverse of the SOC for a certain period or cycle. For example, when the battery has a SOC of 40% it has a DOD of 60%.

The C-rate is the measure at which the battery will discharge entirely. For example, at 1C, the battery will discharge completely in 1 hr.

The internal resistance of a battery cell is dependent on many factors like the temperature, the SoC and the C-rate. Therefore, it cannot be considered constant. This resistance is used to model the voltage drop across the cell and the power dissipated due to this voltage drop.

Lithium ion cell use lithium ions to store and provide energy. It consists of two electrodes with a separator in between. A current collector is put on each electrode, a copper current collector is on the negative side (anode) and aluminum current collector on the positive side (cathode).

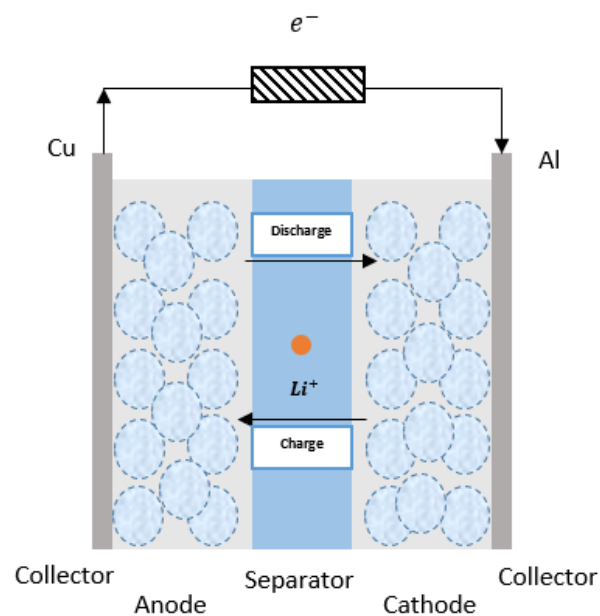


Figure 3.1 Construction of a Li-ion Battery

D. Electrical model

The battery model in this thesis is represented using an electric circuit. The circuit components model the long and short term behavior rather than the electrochemical processes in the cell. The short term models the behavior of the cell over one charging or discharging cycle. Whereas, the long term models the behavior of internal cell impedance over the lifetime of the cell. Note that the battery pack used in this design does not consist of a single cell. Multiple cells are connected in series and in parallel to build the battery pack that fits the required power.

1. Electrical circuit representation

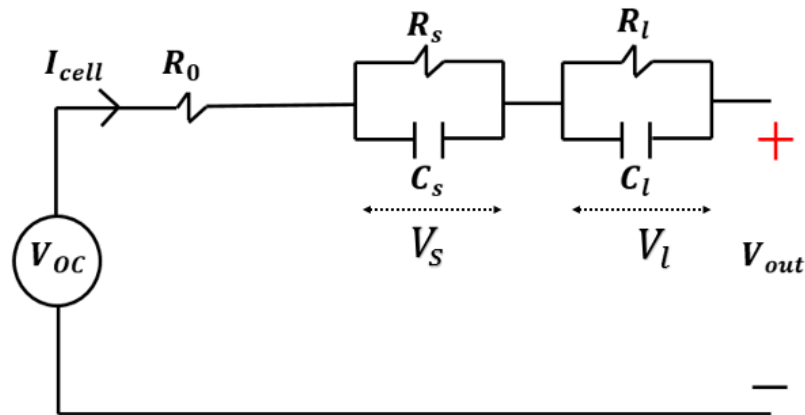


Figure 3.2 Electrical circuit Model

As explained by Long Lam in his master thesis on “A Practical Circuit based Model for State of Health Estimation of Li-Ion Battery Cells in Electric Vehicles” [25], the circuit components are highly nonlinear and are dependent on several factors. Their equations were extracted from measurement data and can be related to the electrochemical processes within the Li-ion.

The equivalent circuit-based model as shown in Figure 3.2 is capable of simulating the performance of Li-ion cell at any instance in time. It contains a dependent voltage or the OCV of the cell, a series resistance (combines the contact resistance, bulk resistance and surface layer resistance), one parallel RC pair with a small time constant symbolizing the charge transfer between two layers, and another parallel RC pair with a long time constant representing the natural movement of particles in the cell. To determine the capacity and parameters for these components, every few cycles a capacity and parameter test cycle were conducted by long lam.

1. Each cell was fully charged to a maximum voltage of 3.6V and rested before a test cycle occurs.
2. In the non-linear voltage region, the cells were discharged at 1C in steps of 0.05 Ah and rested for 1 minute.
3. In the linear voltage region, cells were discharged at 1C in steps of 0.1 Ah before being rested for 1 minute.
4. At the end of the cycle, the cells were rested for 15 minutes before the charging test cycle, which is similar to the discharging test cycle.

Note that during the 1 minute rest interval, the parameters of the circuit were determined at different SOCs.

2. *Open circuit Voltage calculation*

The open-circuit voltage (OCV) is greatly dependent on the SOC and were experimentally determined in a procedure similar to the one explained above. But the cells were rested for 2 hours during each interval rather than 1 minute. Measurements were then

collected at different SOC's and temperatures and fitted in an equation.

The best way to describe the open circuit voltage was found to be an exponential as shown in the below equation. However, the temperature has a very small effect on the open circuit voltage of the battery and is neglected in this work.

$$V_{OC}(SOC) = a_1 e^{-a_2 SOC} + a_3 + a_4 SOC + a_5 e^{-\frac{a_6}{1-SOC}} \quad (3.2)$$

With the OCV as a basis, the rest of the circuit impedances were then extracted.

3. *Circuit impedances calculation*

The values for the internal cell impedances were determined from the step response of the cell voltage during the rest interval which is represented in Figure 3.3.

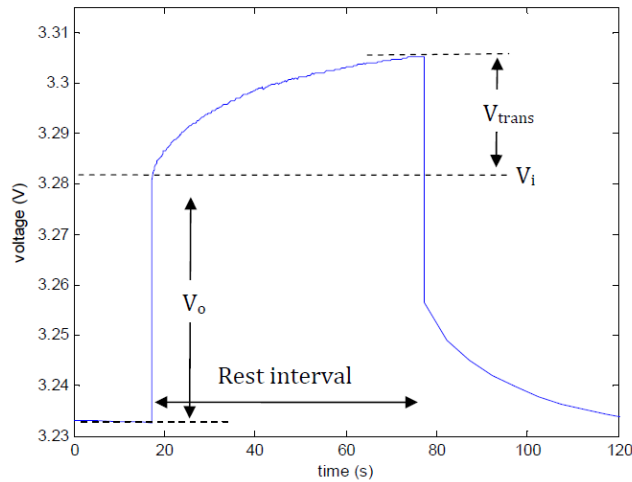


Figure 3.3: Example of a battery voltage during a discharging resting interval

The voltage drop V_0 is the instantaneous voltage drop after the current is cut off which is smaller than one second. I is the current in Amps before the rest interval, and V_{trans} is the voltage response without V_0 .

The circuit impedances were obtained using curve fitting at each rest interval at different SOCs and battery temperatures. The internal cell impedances for discharging is not the same for charging resulting in two sets of equations per impedance. The equations of these impedances are presented in tables 3.2 and 3.3 function of the SOC and temperature for discharging and charging respectively. The parameters for these equations are in tables 3.4, 3.5 and 3.6.

Table 3.2: Discharging Parameters [25]

Discharging series resistance	$R_{0d} = (b_{1d}SOC^4 + b_{2d}SOC^3 + b_{3d}SOC^2 + b_{4d}SOC + b_{5d}). b_{t1d}e^{\frac{b_{t2d}}{T - b_{t3d}}}$
Discharging short transient resistance	$R_{sd} = c_{1d}e^{-c_{2d}SOC} + c_{3d} + c_{4d}SOC + c_{t1d}(T - T_{ref}) + c_{t2d}(T - T_{ref})SOC$
Discharging short transient Capacitance	$C_{sd} = d_{1d}SOC^3 + d_{2d}SOC^2 + d_{3d}SOC + d_{4d} + d_{t1d}(T - T_{ref})SOC + d_{t2d}(T - T_{ref})$
Discharging long transient resistance	$R_{ld} = g_{1d}e^{-g_{2d}SOC} + g_{3d} + g_{4d}SOC + g_{t1d}(T - T_{ref})g_{1d}e^{-g_{2d}SOC} + g_{t2d}(T - T_{ref})$
Discharging long transient Capacitance	$C_{ld} = (h_{1d}SOC^6 + h_{2d}SOC^5 + h_{3d}SOC^4 + h_{4d}SOC^3 + h_{5d}SOC^2 + h_{6d}SOC + h_{7d}). h_{t1d}e^{\frac{h_{t2d}}{T}}$

Table 3.3: Charging Parameters [25]

Charging series resistance	$R_{0c} = (b_{1c}SOC^4 + b_{2c}SOC^3 + b_{3d}SOC^2 + b_{4d}SOC + b_{5d}). b_{t1c}e^{\frac{b_{t2c}}{T-b_{t3c}}}$
Charging short transient resistance	$R_{Sc} = c_{t1c}e^{c_{t2c}T+(c_{t3c}T+c_{t4c})SOC} + c_{t5c}T + c_{t6c}$
Charging short transient Capacitance	$C_{Sc} = d_{1c}SOC^4 + d_{2c}SOC^3 + d_{3d}SOC^2 + b_{4d}SOC + b_{5d} + d_{t1c}(T - T_{ref})$
Charging long transient resistance	$R_{lc} = (g_{lc}e^{-g_{2c}SOC} + g_{3c} + g_{4c}SOC)(g_{t1c}T + g_{t2c})$
Charging long transient Capacitance	$C_{lc} = (h_{1c}SOC^5 + h_{2c}SOC^4 + h_{3d}SOC^3 + h_{4d}SOC^2 + h_{5d}SOC + h_{6c}). h_{t1c}e^{h_{t2c}T}$

Table 3.4: OCV Parameters [25]

a_1	a_2	a_3	a_4	a_5	a_6
5.863E-01	21.9	3.414	1.102E-01	1.718E-01	8E-03

Table 3.5: Impedance Parameters for charging [25]

b1c	1.37E-01	d1c	-1.03E+04	g4c	7.47E-03
b2c	-2.52E-01	d2c	1.72E+04	h1c	-1.54E+05
b3c	1.61E-01	d3c	-1.01E+04	h2c	2.04E+05
b4c	-4.10E-02	d4c	2.34E+03	h3c	-4.01E+03
b5c	8.21E-02	d5c	6.85E+02	h4c	-8.12E+04
c1c	5.90E-10	g1c	8.91E-15	h5c	2.28E+04
c2c	-18.75	g2c	-32.23	h6c	7.14E+03
c3c	1.39E-02	g3c	3.10E-02		
bt1c	7.19E-01	ct3c	-1.18E-01	gt1c	-1.34E-02
bt2c	33.91	ct4c	13.99	gt2c	5.01E+00
bt3c	2.00E+02	ct5c	-1.90E-04	ht1c	2.61E-05
ct1c	9.87E+08	ct6c	7.05E-02	ht2c	3.54E-02
ct2c	-1.48E-01	dt1c	8.814		

Table 3.6: Impedance Parameters for Discharging [25]

b1d	1.30E-01	c4d	-6.46E-03	g4d	-2.42E-02
b2d	-2.89E-01	d1d	1.70E+02	h1d	2.13E+06
b3d	2.27E-01	d2d	-1.01E+03	h2d	-6.01E+06
b4d	-7.22E-02	d3d	1.41E+03	h3d	6.27E+06
b5d	8.98E-02	d4d	3.90E+02	h4d	-2.96E+06
c1d	1.08E-02	g1d	2.95E-01	h5d	6.00E+05
c2d	11.03	g2d	20	h6d	-3.10E+04
c3d	1.83E-02	g3d	4.72E-02	h7d	2.23E+03
bt1d	7.61E-01	ct2d	2.23E-04	gt2d	-5.97E-04
bt2d	1.01E+01	dt1d	-6.58E+00	ht1d	3.13E+03
bt3d	2.61E+02	dt2d	1.21E+01	ht2d	-2.40E+03
ct1d	-3.70E-04	gt1d	6.72E-03		

4. *Total cell voltage*

The battery voltage is then calculated from the above circuit diagram (Figure 2.2) as follows:

$$V_b = V_{oc} - R_o I_b - V_l - V_s \quad (3.3)$$

I_b is the battery current which is negative when charging and positive when discharging. R_o is the series resistance V_s and V_l are the short and long time transient voltage drops. Each transient voltage is calculated using the differential equation that follows:

$$I_b = \frac{V}{R} + c \frac{dV}{dt} \quad (3.4)$$

E. Thermal model

1. Heat Generated

The heat generated (Q_g) in one battery cell is found from the equivalent circuit, where the heat generated is due to the resistances in the circuit. As shown in the following equation, the total heat generated in the battery pack is the number of battery cells(N) times the heat generated per one cell.

$$Q_g = N \left(R_0 * I_b^2 + \left(\frac{V_s^2}{R_s} \right) + \left(\frac{V_l^2}{R_l} \right) \right) \quad (3.5)$$

2. Heat loss to the cooling system

Heat loss in the battery depends mainly on the cooling system, where the pack is coated by an isolating material to prevent the heat from transferring to the passengers' seats. This equation represents the heat lost to cooling system (Q_{cb}) in our model:

$$Q_{cb} = \dot{m}_b c_{lb} (T_{1b} - T_{2b}) \quad (3.6)$$

Where c_{lb} the specific is heat of the coolant, T_{1b} and T_{2b} are the coolant inlet and the outlet temperatures, and \dot{m}_b is the mass flow rate of the cooling liquid inside the battery pack.

3. Temperature of the cell

The final value of the total heat dissipated (Q_c) is obtained by removing the heat loss from the generated heat. Heat lost to the environment via convection and radiation is neglected due to the fact that the battery is placed directly below the passengers' seats so a good insulation material is enclosing the battery back to prevent heat from transferring.

$$Q_c = Q_g - Q_{cb} \quad (3.7)$$

Then the temperature variation in the cell is then found from:

$$m_t C_t \frac{\partial T_{cell}}{\partial t} = Q_c \quad (3.8)$$

F. Results

The open circuit voltage is plotted in Figure 3.4 over the entire SOC interval. Showing a linear region between 0.2 and 0.9 SOC. The circuit impedances for the discharging cycle are presented in Figures 3.5, 3.6, 3.7 and 3.8. The series resistance has a constant value between 0.2 and 0.9 SOC whereas the short transient resistance shows a decrease in its value. On the other hand, the short and long transient capacitances show an overall rise in their values. At higher temperatures, the series and short transient resistances drops, whereas the short and long transient capacitances grow.

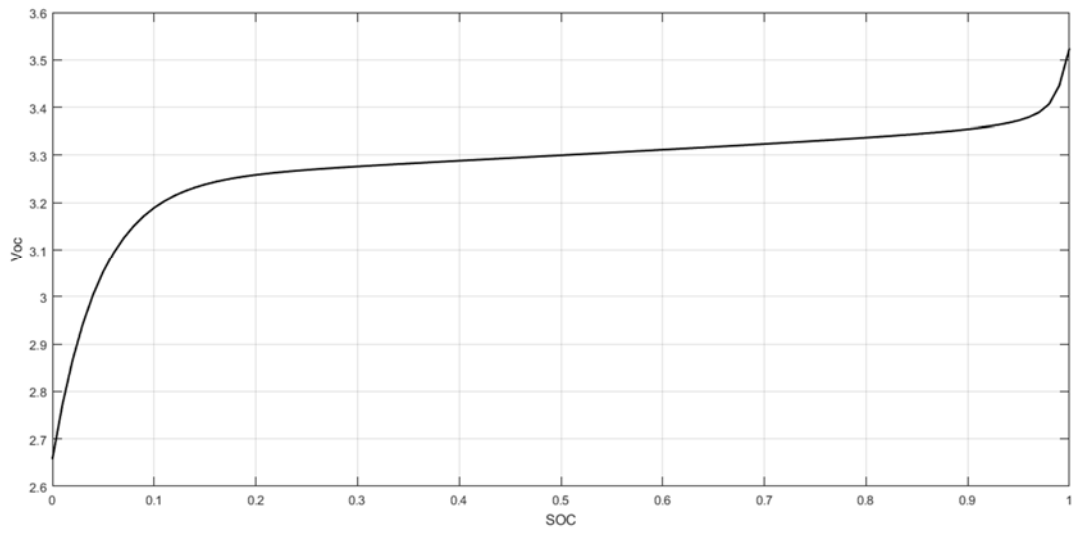


Figure 3.4: Open circuit voltage with respect to SOC

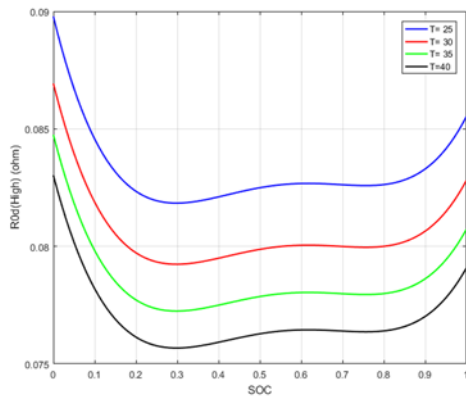


Figure 3.5: Series resistance
resistance

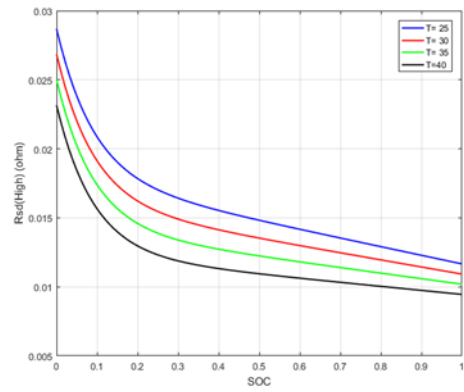


Figure 3.6: Short transient

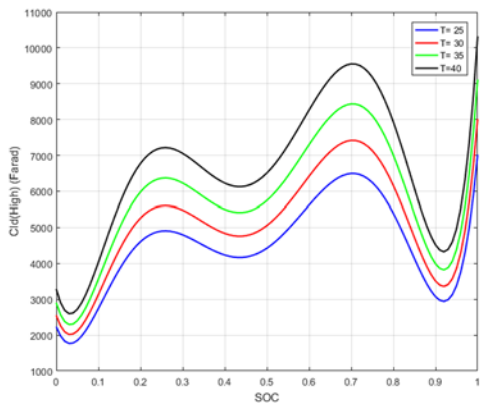


Figure 3.7: Long transient capacitance capacitance

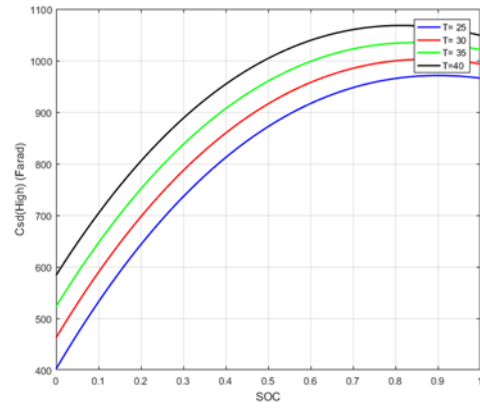


Figure 3.8: Short transient

CHAPTER4

AUXILIARIES AND HYDROGEN TANK

A. Chapter overview

In this chapter we are going to discuss the auxiliary systems in the fuel cell vehicle. It includes the cooling system for the fuel cell and the battery, the humidifier used to keep the fuel cell membrane perfectly humidified for a good performance, and the operation of the compressor needed to compress the air from the environment into the fuel cell. In addition to that, the temperature and pressure variation in the gas tank is being modeled.

B. Cooling system

Excessive fuel cell temperatures for example, can cause the dryness of the membrane (Nafion 115) which relies on liquid water humidification. This implies that temperatures above 90 °C may cause the membrane to dry and hence stop the transportation of protons in the membrane [3, 26].

As for the battery, temperatures higher than the acceptable range may cause a faster degradation rate of the battery. Furthermore, excessive high temperatures may cause a thermal runaway and hence safety issues. To be able to cool the fuel cell and the battery in automotive applications, a cooling system must be build that consists of a radiator, a fan and a pump to circulate the liquid coolant into the fuel cell and the battery. The liquid used in cooling is a blend between water and glycol.

Starting with the radiator, it is made up of flattened aluminum tubes with aluminum strips that zigzag between the tubes. These fins are used to transfer the heat from the liquid in the tubes to the air stream to be carried away from the main system components. In most

modern radiators (Figure 4.1), the tubes run horizontally or vertically with a plastic tank on either side. The radiator frontal area must be large enough to allow the heat transfer from the water to the air [27].

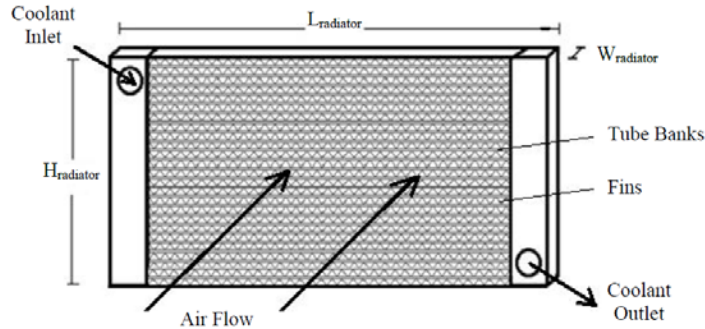


Figure 4.1: The radiator [27]

Connected to the radiator, is an electric water pump. This device will keep the coolant moving as long as the car is running. The water flow from the components must be sufficient to carry the rejected heat to the radiator. Similarly, the water pump must be large enough to handle the required coolant flow rate.

Mounted on the back of the radiator is an electric fans inside a housing that is designed to direct the air flow. The electric fan is controlled by the vehicle's computer, where a sensor will monitor the fuel cell temperature and sends this information to the computer.

The computer then determines if the fan should be turned on or off. The airflow through the radiator must be sufficient to carry away the heat transferred from the liquid coolant.

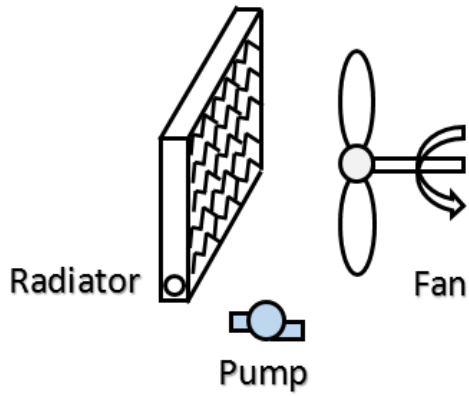


Figure 4.2: Cooling system components

Table 4.1: Specifications of the Cooling System Components [28]

Radiator	
Core (LxWxH)	690 mm 435 mm 26 mm

Fan		Pump	
Type	Pusher	Electric water pump	
Diameter	400 mm	200 l/m	
flow rate	1800 CFM	202.6 kPa	
Power	120 Watt	5000 rpm	

1. The ε -NTU method

To be able to find the amount of heat transferred, output air temperature, and the temperature of the coolant, the ε -NTU method which is based on the concept of heat exchanger effectiveness is used.

The heat capacity rate of air (C_a) and the heat capacity rate of water (C_w) are calculated in the equations below:

$$C_a = m_a C_{pa} \quad (4.1)$$

$$C_w = m_w C_{pw} \quad (4.2)$$

$$C_{min} = \min(C_a, C_w) \quad (4.3)$$

Where” C_{min} ” is the minimum heat capacity rate, “ m_a ” and “ m_w ” are the air and the water mass flow rates.” C_{pa} ” and “ C_{pw} ” are the specific heat capacities of air and water.

The heat capacity rate is the ratio between the minimum and the maximum of C_a and C_w :

$$C_r = \min(C_a, C_w) / \max(C_a, C_w) \quad (4.4)$$

The number of transfer units (NTU) is calculated from the overall heat transfer coefficient (UA):

$$NTU = \frac{UA}{C_{min}} \quad (4.5)$$

The effectiveness of the radiator has the following equation.

$$\varepsilon = 1 - e^{\left[\left(\frac{1}{C_r} NTU \right)^{0.22} \left(e^{-C_r NTU^{0.78}} - 1 \right) \right]} \quad (4.6)$$

The predicted heat transfer is found using equation (4.7) and the outlet temperatures of water ($T_{water,out}$) and air ($T_{air,out}$) are given using equations 4.8 and 4.9 respectively.

$$Q_{predicted} = \varepsilon C_{min}(T_{water,in} - T_{air,in}) \quad (4.7)$$

$$T_{water,out} = T_{water,in} - \frac{Q_{predicted}}{C_w} \quad (4.8)$$

$$T_{air,out} = T_{air,in} - \frac{Q_{predicted}}{C_a} \quad (4.9)$$

C. Humidifier

Water management in PEMFCs is a challenge. For proper operation, and since ionic conductivity in the polymeric membrane is directly related to its water content, membranes must be properly saturated. But, in order to ensure optimum performance, excess water must be removed. The amount of liquid water and membrane humidification levels can be modified by controlling the relative humidity of the reacting gases, as well as their individual pressures and temperatures [26].

Under low temperatures, the amount of water produced by the oxygen half reaction at the cathode is enough for the membrane hydration. However, this fact does not ensure an equilibrium point in water content at high temperatures. In most cases, a gas humidification system is required, at least at the cathode to control the humidity level.

Humidity of air in PEMFC must be carefully controlled. The air entering the fuel cell must be dry enough to evaporate the product water, but not so dry to prevent the dryness of the membrane. It is essential that the electrolyte membrane retains a high water content where the humidity should be above 80% to prevent excess drying, but must be below 100% to prevent the water from collecting at the electrodes [3].

Several methods used to humidify the reactant gases of a fuel cell are available where no standard has yet emerged; some of these methods are discussed below [3]:

- “sparging” is where the fuel cell is humidified by passing the gases through bubbling water whose temperature is controlled.
- Direct injection of water as a spray. This method has an advantage of cooling the reactant gases before entering the fuel cell. It requires the use of pumps and a solenoid valve that opens and closes the injector.
- Another method uses metal foam that makes a kind of water spray to humidify the gases.
- This method was used in the past, where the PEM is humidified directly rather than humidifying reactant gases. Pores are constructed into the fuel cell (usually as a part of the gas diffusion layer). These wicks dip into the water and draw it directly into the PEM.
- The direct inject of water into the FC. This technique is combined with a bipolar plate and a “flow field” design that forces the water out of the cell using the high pressured reactant gases to prevent the flooding of the electrode.
- The use of a rotating piece of water-absorbing material. First, it is put in the path of the exit air where it absorbs water. It is then rotated to be put in the path of the entry air which will dry it out.
- In the self-humidification technique, the electrolyte is modified to retain and produce water. Some hydrogen and oxygen diffuse through the electrolyte

producing water. Although this method consumes some of the fuel, it was proven to improve the performance of the electrolyte.

If external humidification of reactant gases is used before injecting them into the fuel cell. This process can be modeled. Air is said to be fully humidified when the partial pressure of water (P_w) and the saturation vapor pressure (P_{sat}) are equal. The air relative humidity (ϕ) is the ratio between these pressures. In dry climates, ϕ is around 30%. As for normal climates, ϕ becomes around 70%.

$$\phi = \frac{P_w}{P_{sat}} \quad (4.10)$$

The saturated vapor pressure depends on temperature and is represented in table 4.2 below:

Table 4.2: Saturated Vapor Pressure of Water at Different Temperatures [3]

T(°C)	Saturated vapor pressure (kPa)
15	1.705
20	2.338
30	4.246
40	7.383
50	12.35
60	19.94
70	31.19
80	47.39
90	70.13

If the exit gas was used to humidify the inlet air, and the water content of the inlet air is not negligible. The following equations are to be used:

$$P_w = \frac{(0.42 + \psi\lambda)P_{exit}}{(1 + \psi)\lambda + 0.21} \quad (4.11)$$

Where " P_w " is the water pressure at the exit, " P_{exit} " is the total pressure at the exit, " λ " is

the air stoichiometry, and “ Ψ ” is defined as follows:

$$\Psi = \frac{P_{win}}{P_{in} - P_{win}} \quad (4.12)$$

Here “ P_{in} ” is the total inlet air pressure, which will usually be a little larger than “ P_{exit} ”, and “ P_{win} ” is the water vapor pressure at the inlet.

D. Compressor model

The system when pressurized helps in the humidification process of the fuel cell, and for temperatures above 80°C it becomes difficult to arrange a proper humidification system at low pressures. The hydrogen gas is already pressurized in the hydrogen tank, so only a regulator valve is needed to decrease the hydrogen pressure at the anode. The case differs for oxygen gas at the cathode, where oxygen is being supplied from the atmosphere and it needs to be pressurized. This is done using a compressor, where the air mass flow is compressed from the atmosphere to reach the operating pressure.

To calculate the power consumption of the compressor (P_{comp}), the following equation was used [3]:

$$P_{comp} = \frac{C_p T_a}{\eta_c} \left[\left(\frac{P_{out}}{P_{in}} \right)^{\frac{\gamma-1}{\gamma}} - 1 \right] \dot{m}_{air} \quad (4.13)$$

Where “ C_p ” is the specific heat, “ T_a ” is the ambient temperature, “ η_c ” is the efficiency of the compressor, “ P_{in} ” and “ P_{out} ” are the input and output pressures, γ is the ratio of the specific heat capacities of the gases, and “ \dot{m}_{air} ” is the air flow rate from the compressor [3].

$$\dot{m}_{air} = \frac{Num I_c}{4F_C 0.21} \lambda_{cathode} \quad (4.14)$$

E. Hydrogen tank model

Hydrogen is the lightest of all elements and the most abundant one in the universe. It can be stored at high pressure in an empty tank, in a liquefied hydrogen storage, or in a tank containing solid. Compressing hydrogen is relatively simple and cost efficient. This is why, most hydrogen storage tanks are based on high pressure vessels.

1. Pressure variation

The Peng-Robinson equation of state is a widely used equation in the industry to describe the pressure, volume and temperature behavior of the real non-ideal gases.

$$P = \frac{RT}{v-b} - \frac{a\alpha}{v^2+2bv-b^2} \quad (4.15)$$

Where v is the molar volume, a and b are calculated as follows:

$$a = 0.45724 \frac{R^2 T_c^2}{P_c} \quad (4.16)$$

$$b = 0.0778 \frac{RT_c}{P_c} \quad (4.17)$$

$$\alpha = \left[1 + k \left(1 - \left(\frac{T}{T_c} \right)^{0.5} \right) \right]^2 \quad (4.18)$$

$$k = 0.37464 + 1.54226 \omega - 0.26992 \omega^2 \quad (4.19)$$

T_c and P_c are the critical temperature and pressure, ω is the acentric factor which differs between gases. For hydrogen ω is equal to -0.22.

2. *Temperature variation*

Since the change of internal energy in the tank is due to the consumption of hydrogen gas from the tank during car operation. The temperature of the gas tank was calculated based on the following equation:

$$(m_0 - m)C_v \frac{dT}{dt} = \dot{m}(C_v - C_p)T \quad (4.20)$$

Where m_0 the initial mass of hydrogen in the tank is, m is the total mass of hydrogen consumed, and \dot{m} is the hydrogen consumption in kg/s. C_v and C_p are the specific heat of hydrogen inside and outside of the tank respectively.

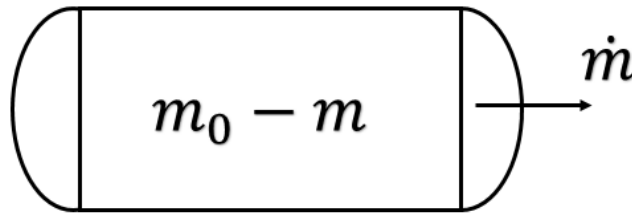


Figure 4.3: Hydrogen tank schematic

CHAPTER 5

SYSTEM INTEGRATION

A. Model integration

1. Introduction

After discussing each element alone, it is time to combine them together in the vehicle. As it is shown in Figure 5.1, the fuel cell is mounted in the front under the cap of the vehicle. The battery on the other hand is placed underneath the seats. Each of these two components have different operating temperatures, so two separate cooling systems are needed. The cooling system includes the radiator, the cooling pump, and the cooling fan. The coolant used here is a mixture between water and glycol. Glycol is an anti-freeze substance which is usually added to prevent the water from freezing at low temperatures.

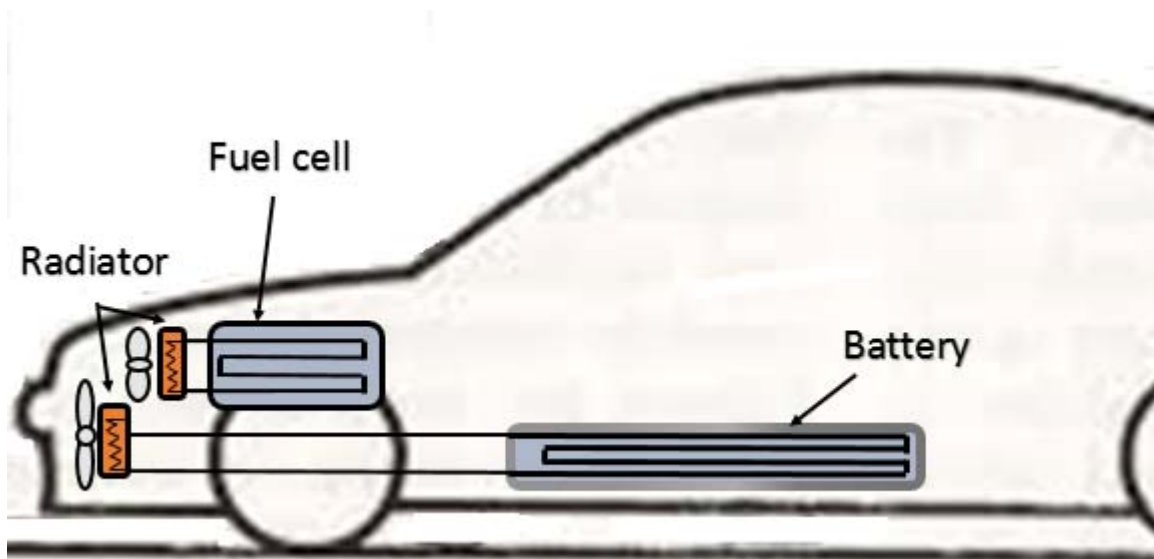


Figure 5.1: Components integration in the vehicle

2. *Fuel cell stack Assembly*

Figure 5.2 shows a single cell assembly. Each cell consists of a cathode and an anode with a membrane in between. The anode is where hydrogen is fed from the hydrogen tank. The cathode is where oxygen is fed from the atmosphere. The electrodes contain staggered channels where the gases pass through.

As it is shown in the figure, the electrodes are voided. These voids or the cooling channels are designed to let the liquid pass through them. To fit the energy requirements of the vehicle, multiple cells must be connected in series and in parallel to form a stack (Figure 5.3). The fuel cell stack is then enclosed on both of its ends.

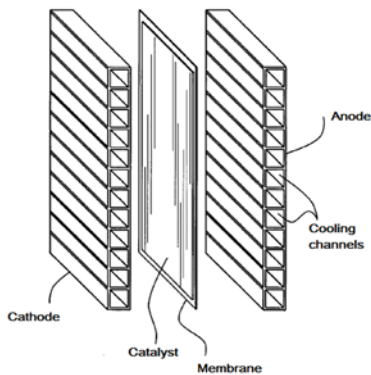
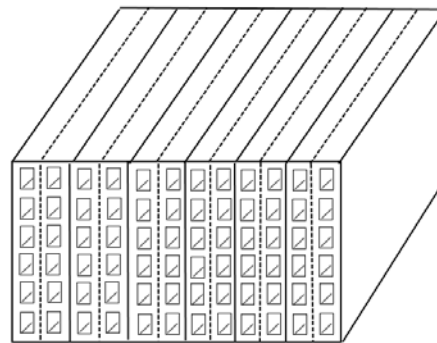


Figure 5.2: Single FC assembly
5.3: FC stack



Figure

Liquid cooling of the FC happens through the radiator whose main purpose is to cool down the inlet water coming into the fuel cell. Figure 5.4 shows a schematic diagram of the fuel cell-cooling system arrangement. In this design, the pump keeps circulating the liquid as long as the car is running. The fan on the other hand, turns on when the

temperature of the fuel cell rises above a certain value.

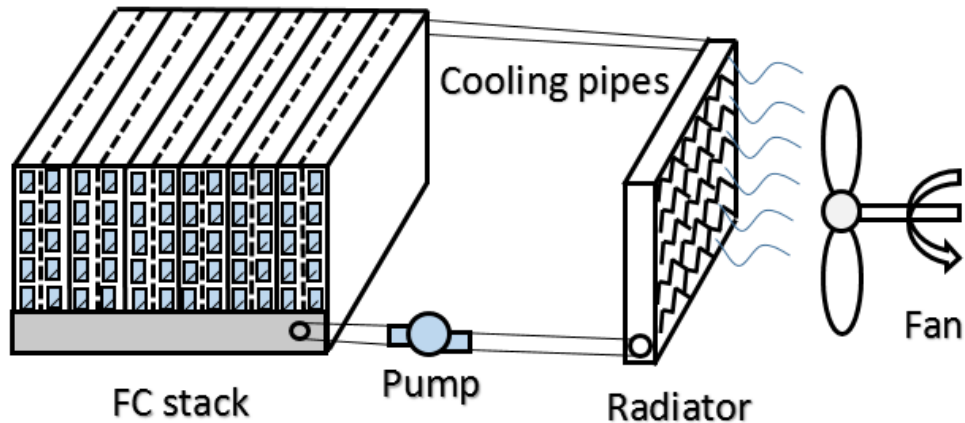


Figure 5.4: FC-cooling system

3. Battery Pack Assembly

The battery cell (Figure (5.5)) used in this design is Lithium iron phosphate (LiFePO_4). Each cell has a charge capacity of 1.1Ah and a maximum voltage of 3.6V. A single cell is not enough to cover the total demand of the vehicle, so multiple cells must be connected in series (Figure 5.6) and in parallel (Figure 5.7). The below Figures were taken from A123 systems battery pack design.

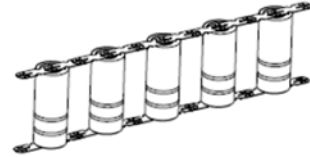
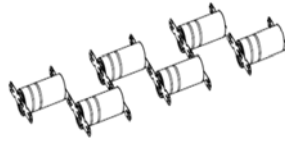
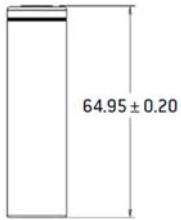


Figure 5.5: Battery cell Figure 5.6: series battery cells Figure 5.7: parallel battery cells

Series and parallel combinations of the cells form a module as it is shown in Figure 5.8. An aluminum cover then encloses the batteries in a single module. This arrangement was done in Tesla cars (models S and X). To be able to control the thermal effect of the battery pack, a cooling channel which contains several voids is inserted between the battery cells in each module as it is shown in Figures 5.8 and 5.9. It passes between the cells in a way that all the cells are in contact with it. The modules are then connected in series to reach the required battery power.

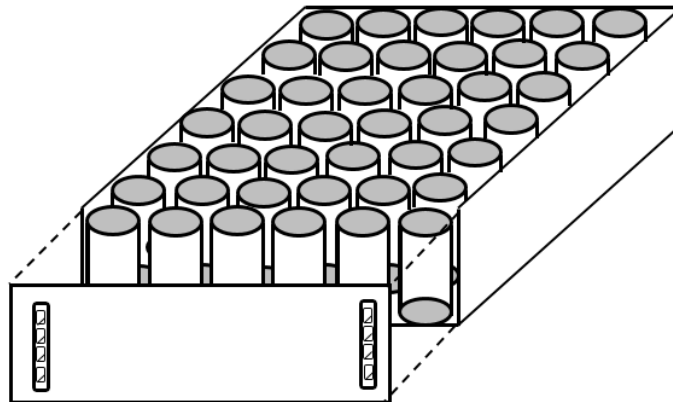


Figure 5.8: battery module

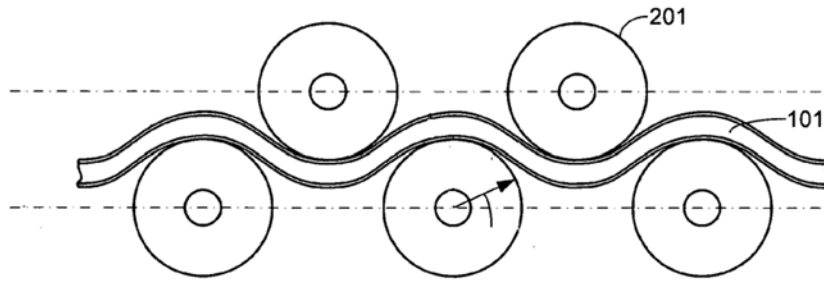


Figure 5.9: cooling channels in the battery module

B. Energy management system

The Energy management system is used to distribute the power between the fuel cell and the battery. To do so, the following steps are adopted:

1. Determine the preferred battery power, $P_b(t)$ based on SOC as given in Figure 5.10. According to the SOC of the battery, its power is determined as follows:

If $SOC \geq SOC_{max}$ then $P_b(t) = P_{b,max}$

If $SOC \leq SOC_{min}$ then $P_b(t) = P_{b,min}$

Else, $P_b(t) = \varphi(SOC(t))$

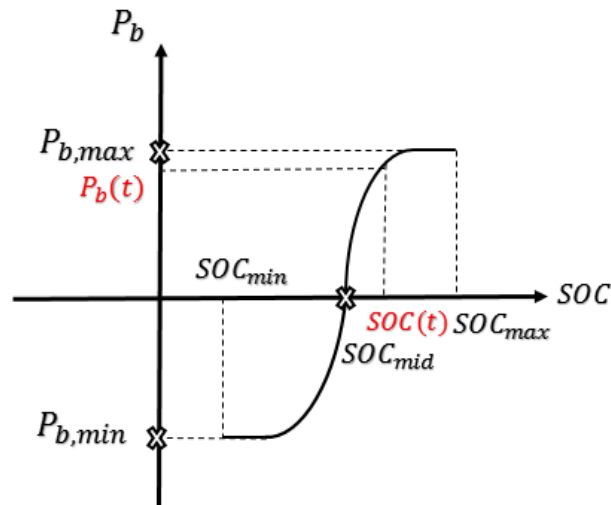


Figure 5.10: Battery required power vs. SOC

2. Determine the change in power in the vehicle Δp .

$$\Delta p(t) = P_d(t) - P_d(t - 1)$$

3. The EMS differentiates between three modes (motoring, generating, and idling), and based on the present mode the system operates as in Figure 5.11.

If $P_d(t) > 0$ –The system is in the motoring mode

If $\Delta p(t) > 0$

$$P_{fc} = \min(P_d(t) - P_b(t), P_{fc}(t - 1) + \Delta P_{fc}, \max P_{fc})$$

$$P_{fc} = \max(P_{fc}, \min P_{fc})$$

If $\Delta p(t) \leq 0$

$$P_{fc} = \max(P_d(t) - P_b(t), P_{fc}(t - 1) - \Delta P_{fc}, \min P_{fc})$$

$$P_{fc} = \min(P_{fc}, \max P_{fc})$$

If $P_d(t) < 0$ –The system is in the generating mode

$$P_{fc} = \max(P_d(t) - P_b(t), P_{fc}(t - 1) - \Delta P_{fc}, \min P_{fc})$$

If $P_d(t) = 0$ –The system is in the idling mode

$$P_{fc} = \max(P_{fc}(t - 1) - \Delta P_{fc}, \min P_{fc})$$

$$P_b = \max(-P_{fc}, \min P_b)$$

4. Check the error in power (e) in every time step:

$$e = P_d(t) - (P_b(t) + P_{fc})$$

If the error is positive, increase the battery power.

If the error is negative, decrease the battery power and set the brake power = $-e$

CHAPTER6

MODEL VALIDATION AND TESTS RESULTS

A. Introduction

Now that we explained the development of a complete vehicle model it is time to simulate it under different driving conditions. To do so, two speed profiles will be used to test the vehicle model, which are the Urban Dynamometer Driving Schedule (UDDS) and Highway Federal Emission Test (HWFET) obtained from the EPA Federal Test Procedure.

The fuel cell and battery were sized to fit the power ratings of a vehicle with a 20 mile battery capacity (FCHEV 20) and another with a 40 mile battery capacity (FCHEV 40). These two vehicle sizes were then used to validate the EMS against the Dynamic programming method. After that the two cars along with an all-battery model were simulated at different inclination angles, different battery operating modes, and different ambient temperatures.

Finally, we will have a close look at what is happening inside each component during the car operation.

B. Speed profile

The developed model was tested under two different speed profiles which are presented in Figures 6.1 and 6.2. One is for a typical urban road (UDDS) and another for a highway road (HWFET).

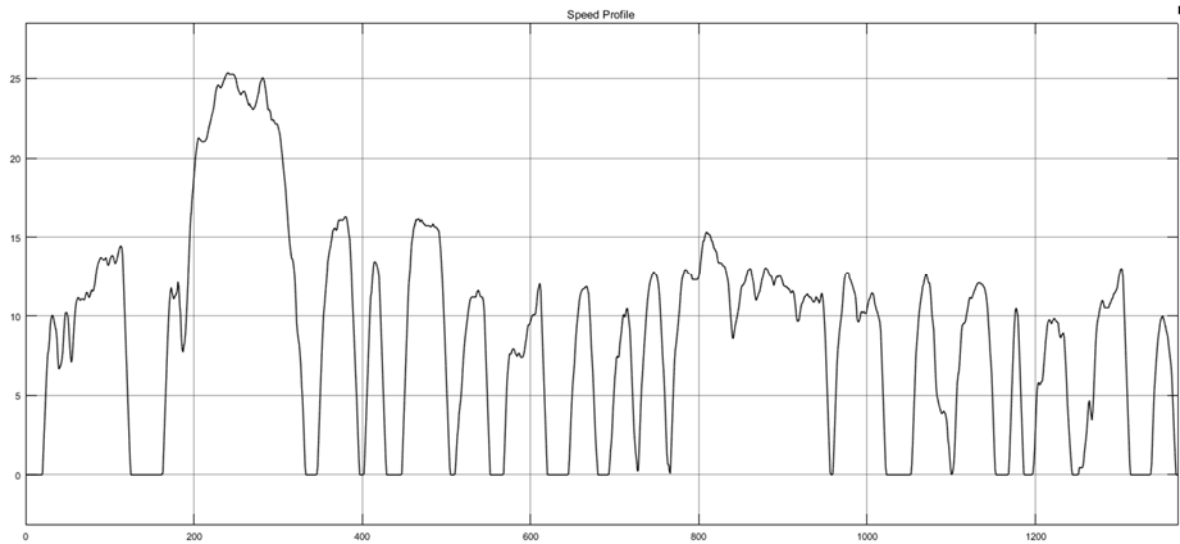


Figure 6.1: Speed profile for an urban road (UDDS)

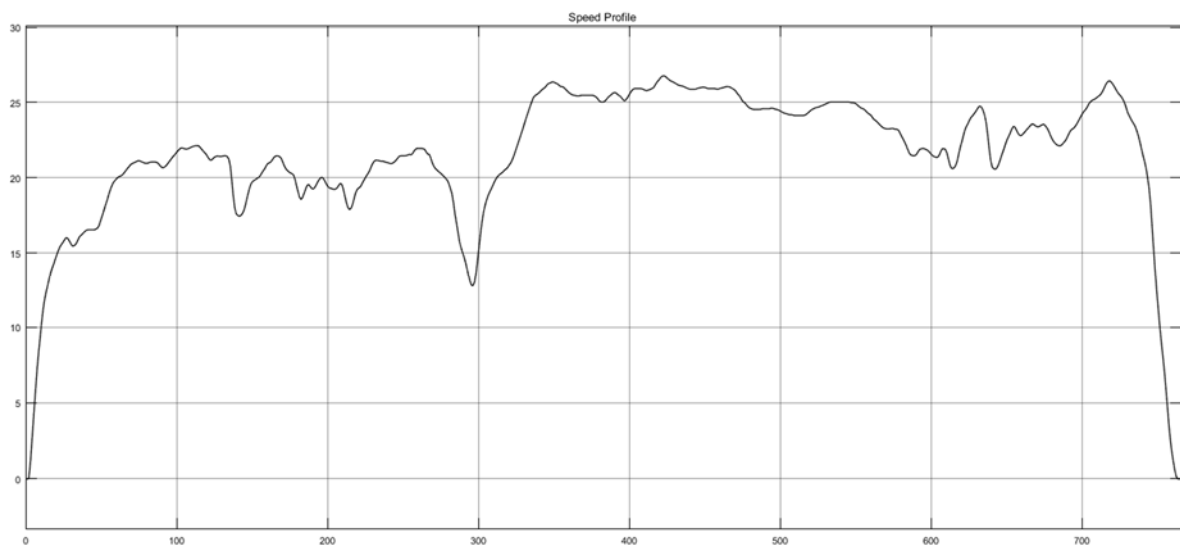


Figure 6.2: Speed profile for a highway road (HWFET)

C. Car sizes

Two cars with two different power ratings for the fuel cell and the battery are going to be tested with the above speed profiles. The fuel cell and the battery specifications are presented in Table 6.1. The car specifications are in Table 6.2, while the car mass distribution is in Table 6.3.

Table 6.1: Fuel cell and Battery Specifications

	Car1: FCHEV 20	Car2: FCHEV 40
Fuel cell		
Maximum Power (kW)	58.8	56.7
Minimum Power (kW)	2.94	2.83
Number of cells in series/string	245	211
Number of strings	2	2
Mass	275.2	265.5
Battery		
Maximum Power (kW)	53	146.8
Minimum Power (kW)	-27.34	-74
Maximum SOC (pu)	0.9	0.9
Minimum SOC (pu)	0.2	0.2
Energy Capacity (kWh)	7.9	17.5
Number of cells in series	6	6
Number of cells in parallel	74	74
Number of modules	4.5	10
Mass	143.9	312.8

Table 6.2: Car Specifications [16]

Air drag coefficient	0.28
Coefficient 0 of rolling resistance	0.005
Coefficient 1 of rolling resistance	0.00023
Wheel radius	0.317
Voltage at the high level	380
Frontal area in square m	2.18
Efficiency of electric motor and inverter when driving	0.9025
Efficiency of electric motor and inverter when braking	0.8
Motor drive Line Efficiency	0.9

Table 6.3: Car Mass Distribution [29]

Body in white(primary vehicle structure)	250.5
Body panels(such as the hood, roof, deck lid, doors, quarter panels, and fenders)	80
Front/Rear bumpers(Impact bars, energy absorbers, and mounting hardware)	10
Miscellaneous components	10
Blanks and fasteners	20
Glass(Front windshield, rear windshield, and door and windows)	40
Exterior	33.6
Interior	171.3
Transmission system(Gearbox, Torque converter, Controls)	37.7
Chassis	332.7
Motor	55.5
Inverter	48.6
Auxiliaries(Including H2 Tank system, Water supply system, air supply system, cooling system, and piping system)	248.2
Total body weight in kg	1338

D. Model validation

Car1 which has a 20 mile battery range is going to be compared with a dynamic programming method. The comparison is done under both driving cycles (UDDS and HWFET) and when the battery is operating in a charge sustaining (CS) or in a charge depletion mode (CD).

Table 6.4: Rule Base versus DP—Charge Depletion Mode

Energy Demand Power Input (kWh)= 1.4385		
FCHEV 20		
	Dynamic Programming	Rule Base
Car Total H2 Consumption (g)	19.43	64.12
Energy Supplied By Fuel Cell (kWh)	0.22	1.12
Energy Supplied By Battery (kWh)	1.35	0.31
Total Energy delivered (kWh)	1.58	1.42
FC Energy delivered/kg of hydrogen (kWh/kg)	11.51	17.45
Total car energy delivered/kg of hydrogen(kWh/kg)	81.3	22.23

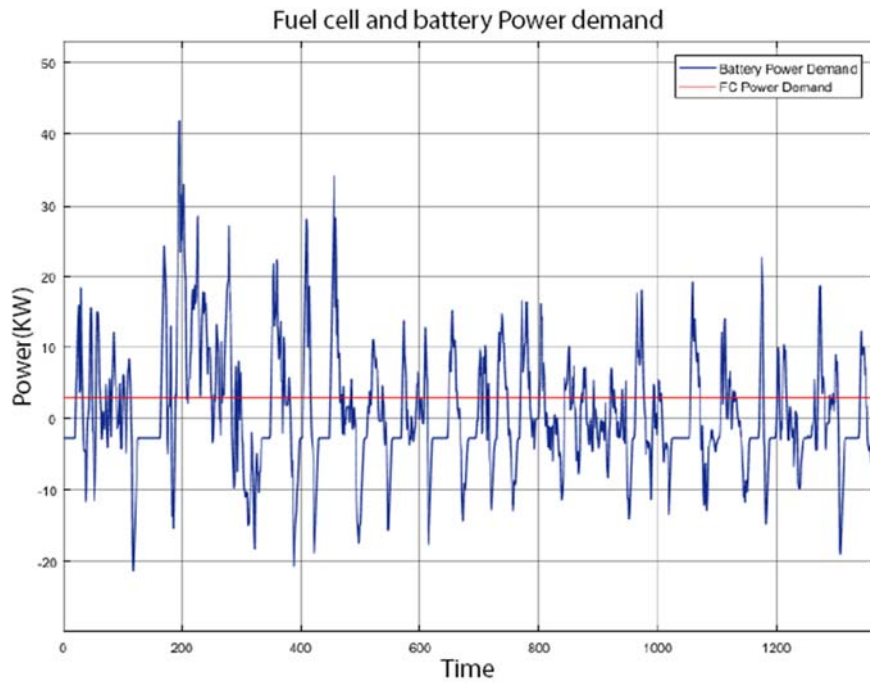


Figure 6.3(a) Rule base power demand

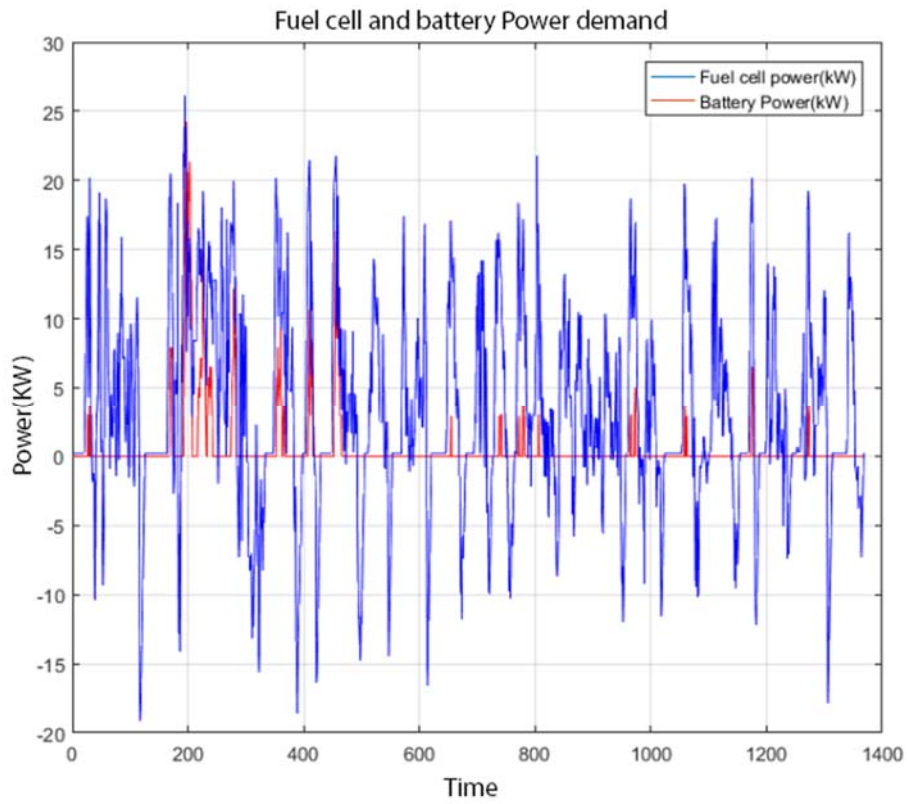


Figure 6.3(b) DP power demand

Figures 6.3(a) and 6.3(b) show the battery and fuel cell power demand in both energy management systems. In Rule base EMS the fuel cell power is kept around the minimum value with an aim to reduce the hydrogen consumption. As for the DP program, it is operating and shutting down the fuel cell in rapid bursts which may not be possible in real system if the minimum startup time and minimum shutdown time are to be observed. The DP may show a better fuel utilization, yet it may not reflect a realistic operating condition.

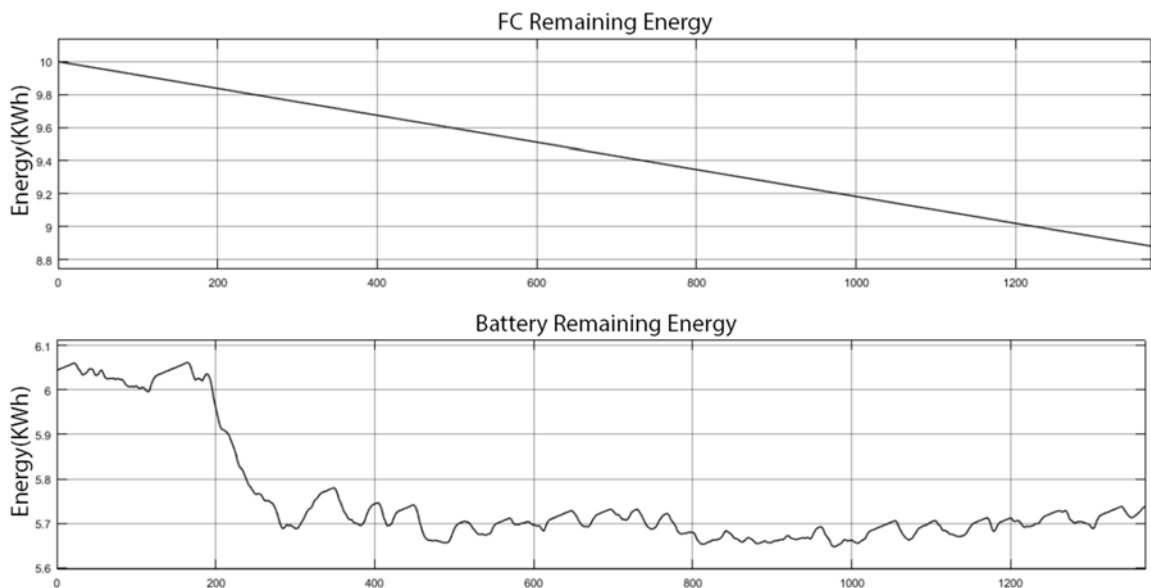


Figure 6.4(a) Fuel cell and battery remaining energy in Rule base

Figure 6.4(b) Fuel cell and battery remaining energy in DP

Comparing Figures 6.4(a) and 6.4(b), it can be seen that in the rule base approach is relying more on the fuel cell rather than the battery. This is due to the continuous operation of the fuel cell.

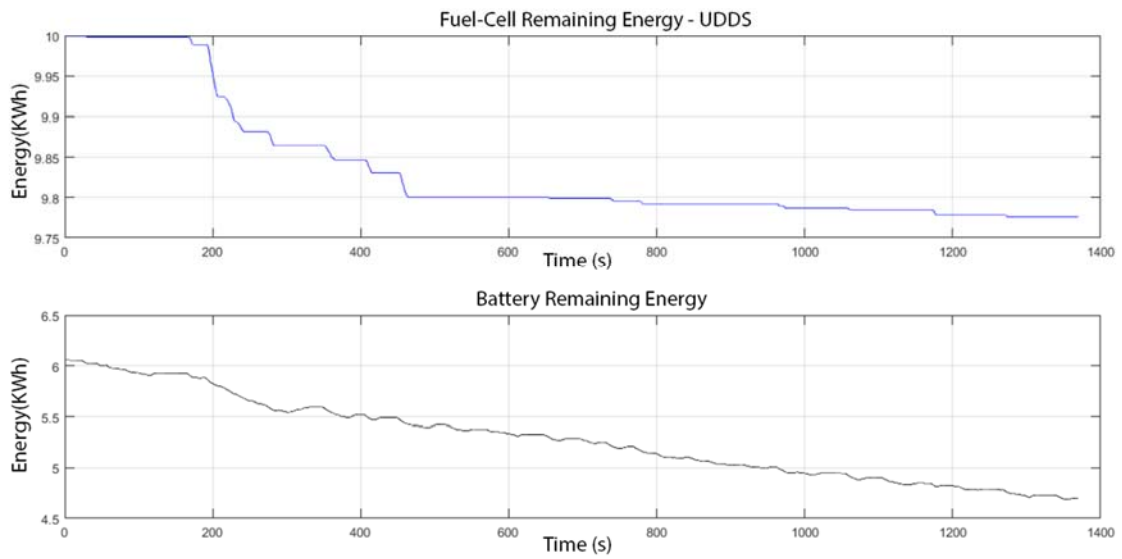


Table 6.5: Rule Base versus DP—Charge Depletion Mode-HWFET

Energy Demand Power Input (kWh)= 2.1529		
FCHEV 20		
	Dynamic Programing	Rule Base
Car Total H2 Consumption (g)	48.32	35.87
Energy Supplied By Fuel Cell (kWh)	0.815	0.62
Energy Supplied By Battery (kWh)	1.45	1.52
Energy delivered	2.26	2.14
FC Energy delivered/kg of hydrogen (kwh/kg)	16.87	17.44
Total car energy delivered/kg of hydrogen(kwh/kg)	46.91	59.84

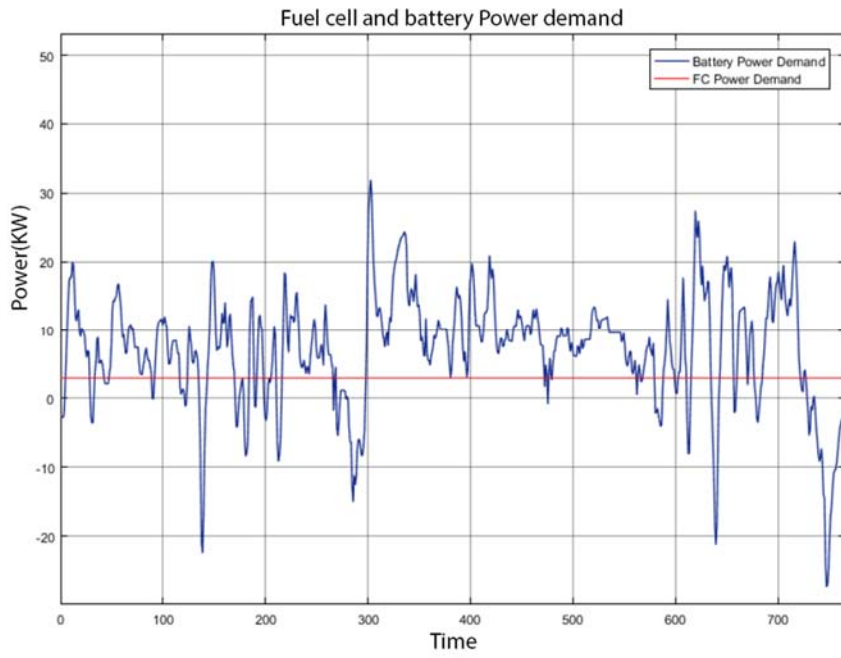


Figure 6.5(a) Rule base power demand

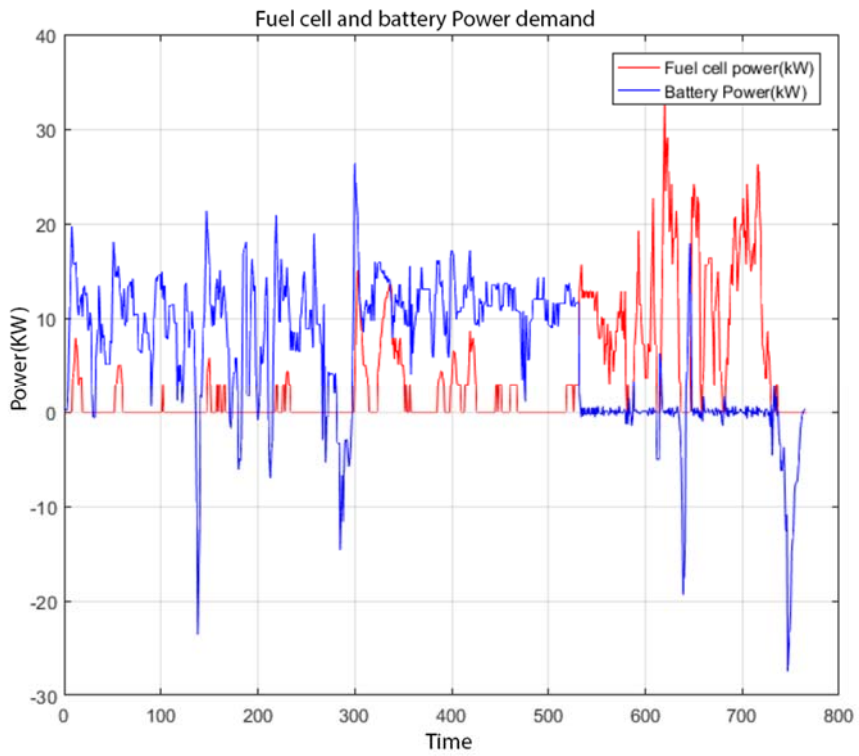


Figure 6.5(b) DP power demand

During this cycle, the fuel cell supplied less energy in rule base than DP. This is because the battery in the DP program reached the mid SOC, so now the battery is on charge sustaining mode and the fuel cell had to fill the gap in the power demand. While in Rule base the mid SOC took longer to be reached due to the excess power provided by the fuel cell that was used in recharging the battery. This is clearly seen in Figures 6.6(a) and 6.6(b).

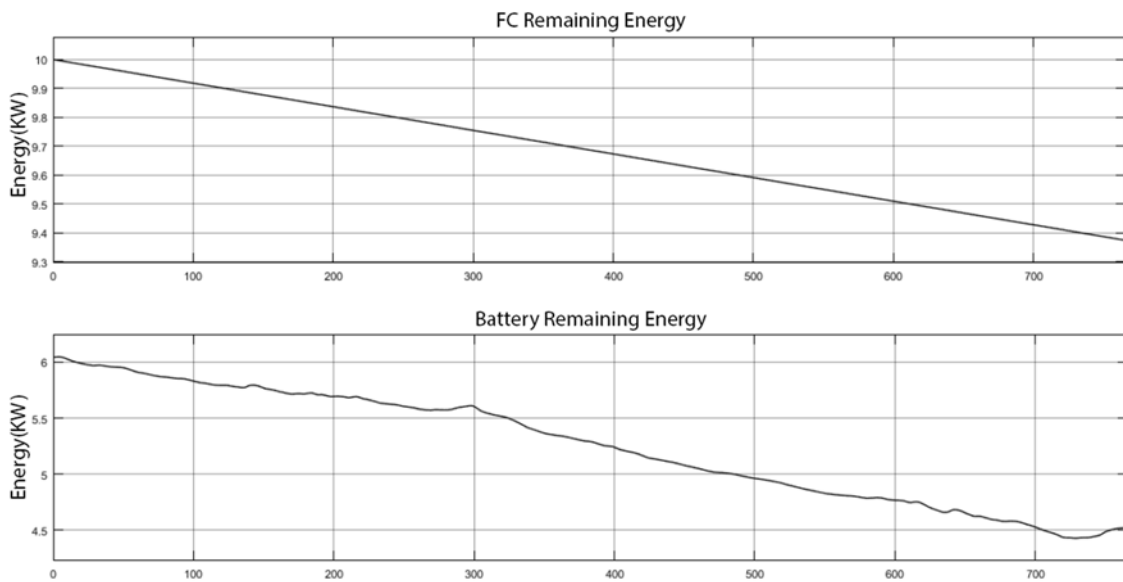


Figure 6.6(a) Fuel cell and battery remaining energy in Rule base

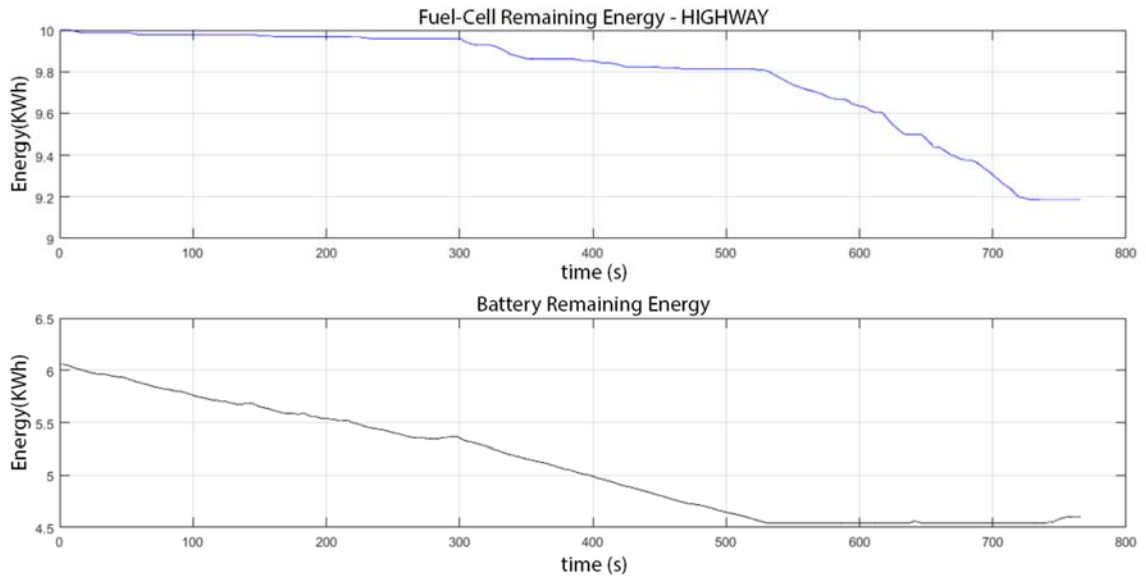


Figure 6.6(b) Fuel cell and battery remaining energy in DP

Table 6.6: Rule Base versus DP—Charge Sustaining Mode-UDDS

Energy Demand Power Input (kWh)=1.52		
FCHEV 20		
	Dynamic Programing	Rule base
Car Total H2 Consumption (g)	89.37	93.9
Energy Supplied By Fuel Cell (kWh)	1.5	1.56
Energy Supplied By Battery (kWh)	-0.01	-0.13
Energy delivered	1.49	1.42
FC Energy delivered/kg of hydrogen (kwh/kg)	16.84	16.62
Total car energy delivered/kg of hydrogen(kwh/kg)	16.7	15.15

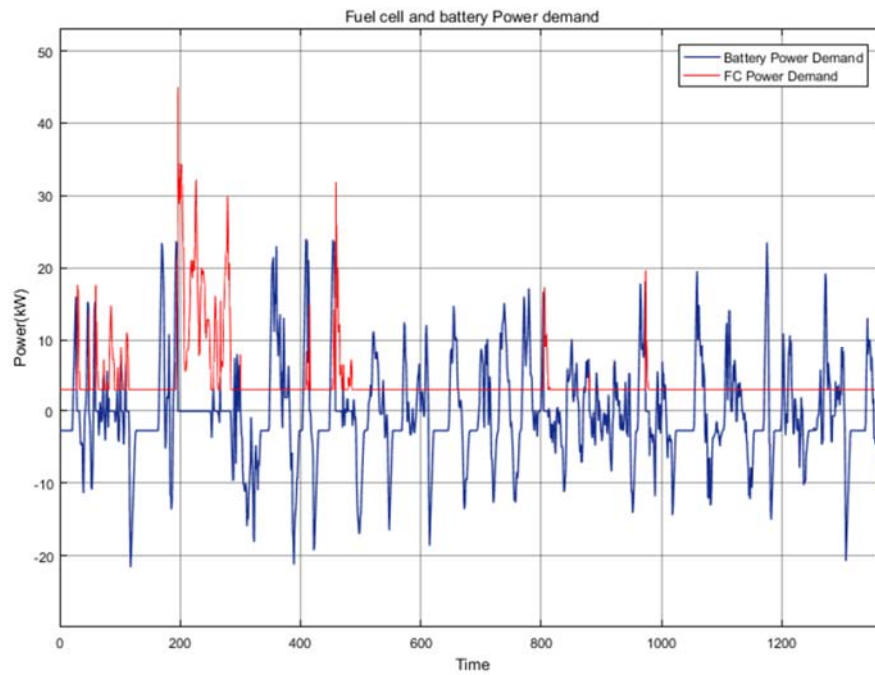


Figure 6.7(a) Rule base power demand

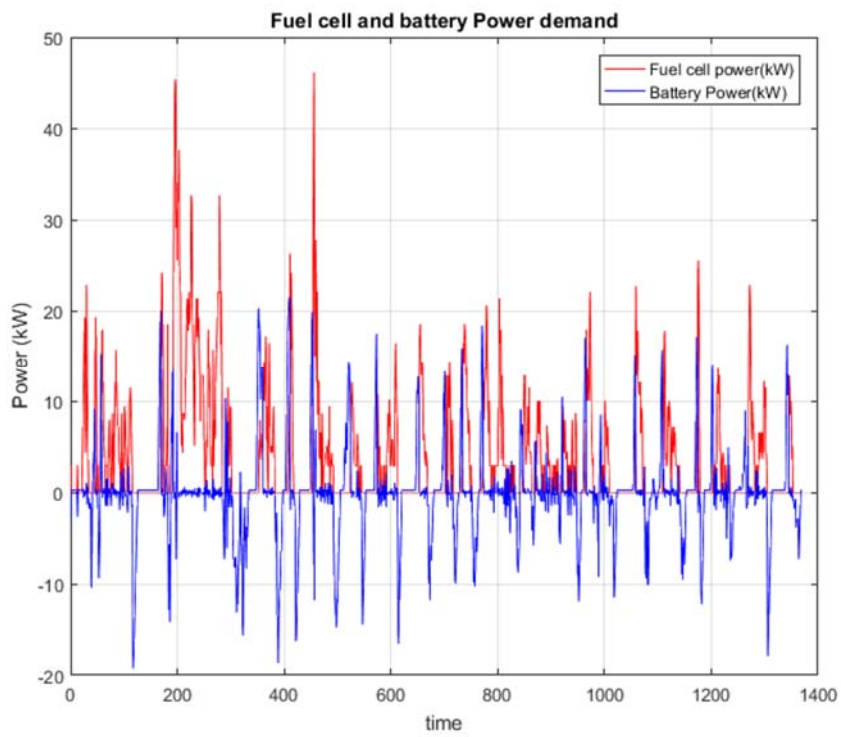


Figure 6.7(b) DP power demand

In the charge sustaining mode, the energy supplied by the two systems is close. The fuel cell is still supplying slightly more energy in Rule base which is charging the battery as it is shown in Figure 6.8(a). This can be referred to the temperature effect. It can be seen that when we take into consideration the temperature the FC consumes more hydrogen for the same amount of energy. Which means that the fuel cell efficiency will decrease. A **4.8** % error in hydrogen consumption was detected when temperature was taken into consideration.

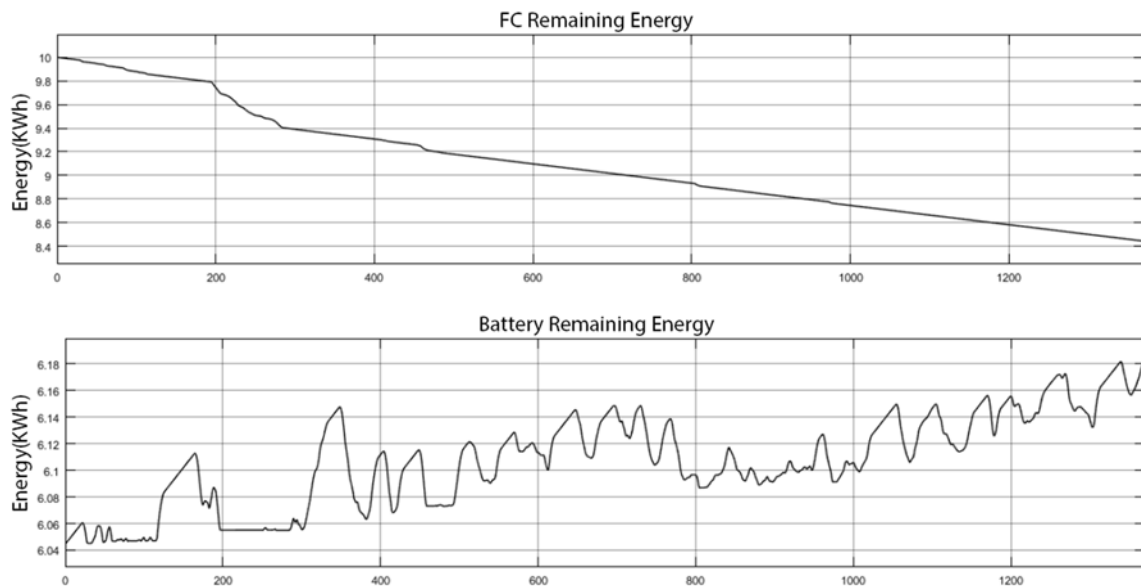


Figure 6.8(a) Fuel cell and battery remaining energy in Rule base

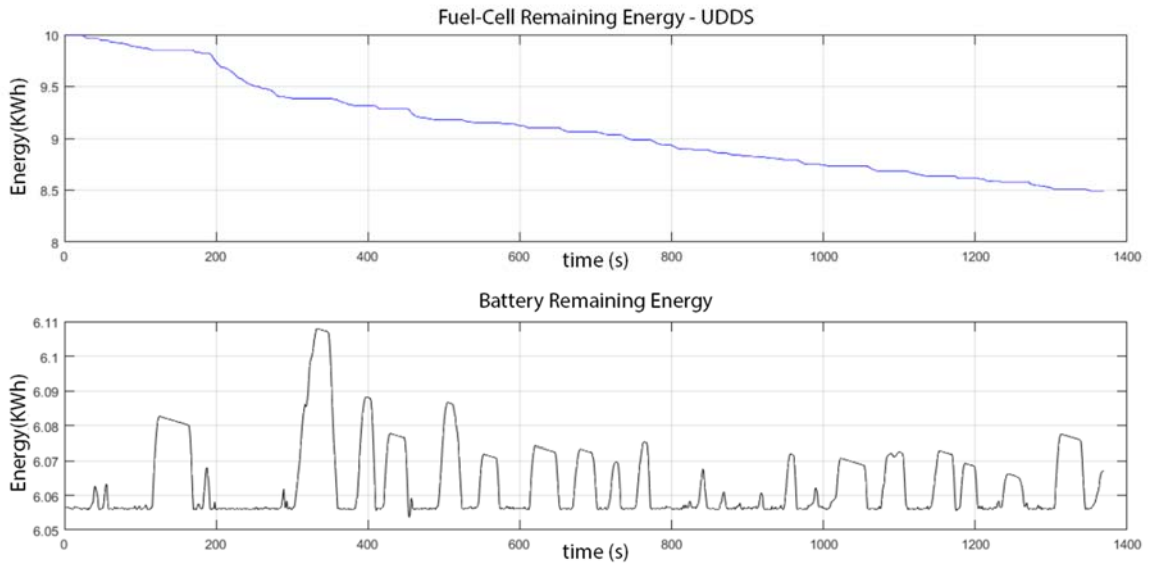


Figure 6.8(b) Fuel cell and battery remaining energy in DP

Table 6.7: Rule Base versus DP—Charge Sustaining Mode-HWFET

Energy Demand Power Input (kWh)= 2.153		
	Dynamic Programing	Rule Base
Car Total H2 Consumption (g)	125.50	144.9
Energy Supplied By Fuel Cell (kWh)	2.23	2.24
Energy Supplied By Battery (kWh)	-0.06	-0.10
Energy delivered	2.16	2.14
FC Energy delivered/kg of hydrogen (kwh/kg)	17.77	15.52
Total car energy delivered/kg of hydrogen(kwh/kg)	17.28	14.78

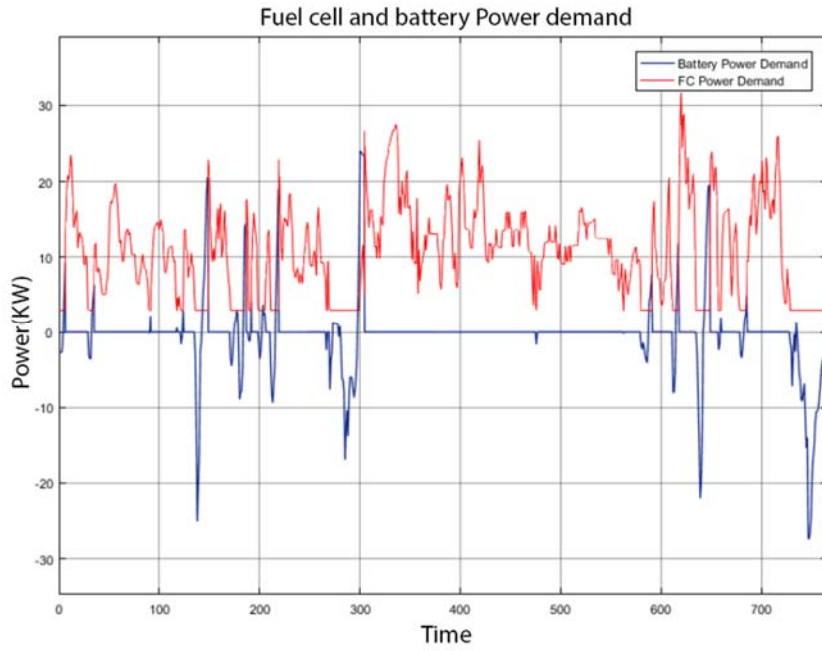


Figure 6.9(a) Rule base power demand

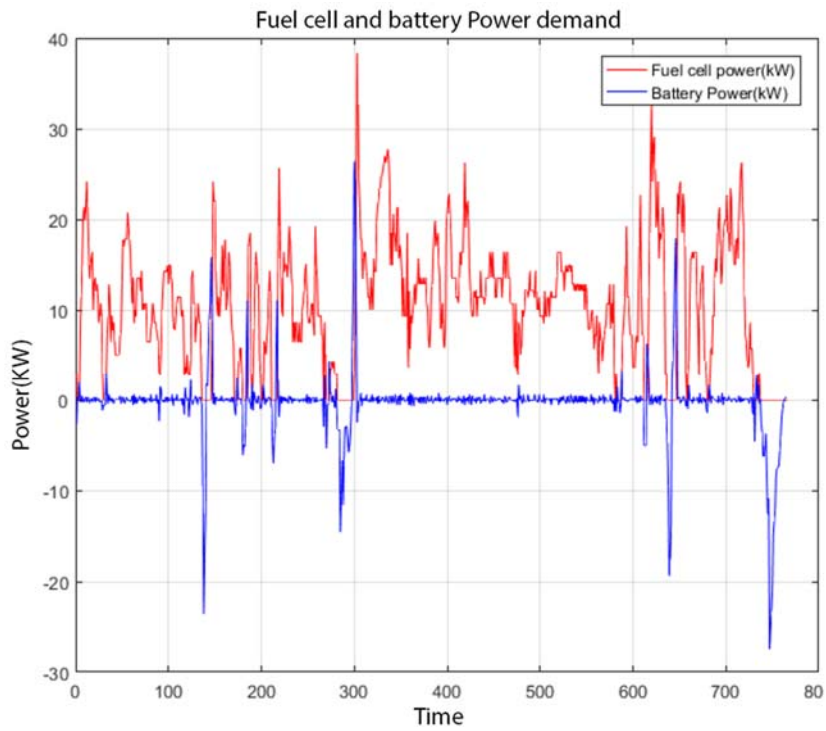


Figure 6.9(b) DP power demand

During the highway driving cycle, the battery is still charging more in the Rule base. But comparing HWFET and UDDS during CS mode, the rule base is closer to DP in HWFET.

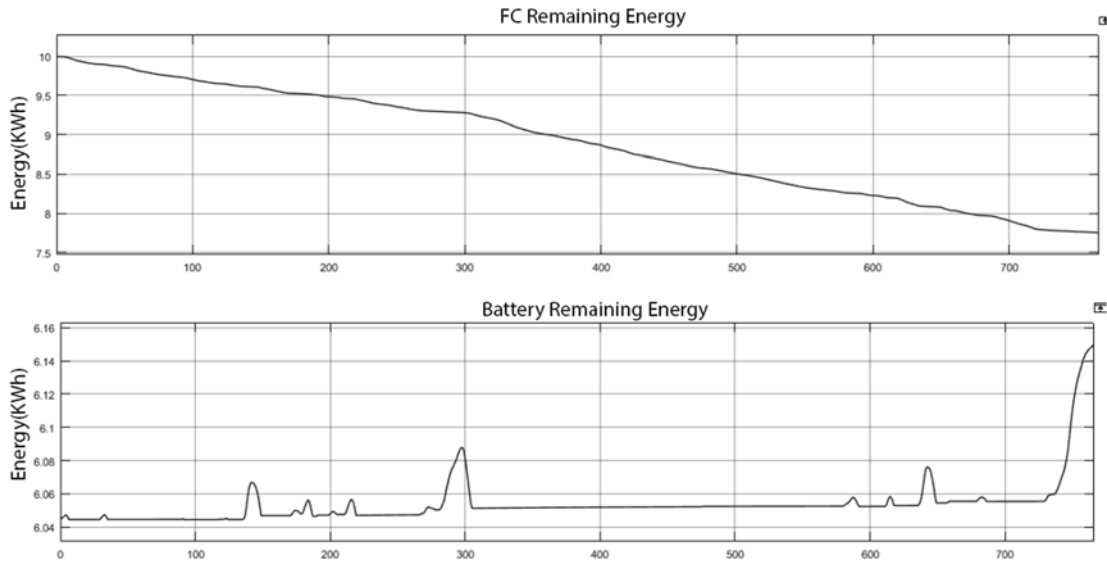


Figure 6.10(a) Fuel cell and battery remaining energy in Rule base

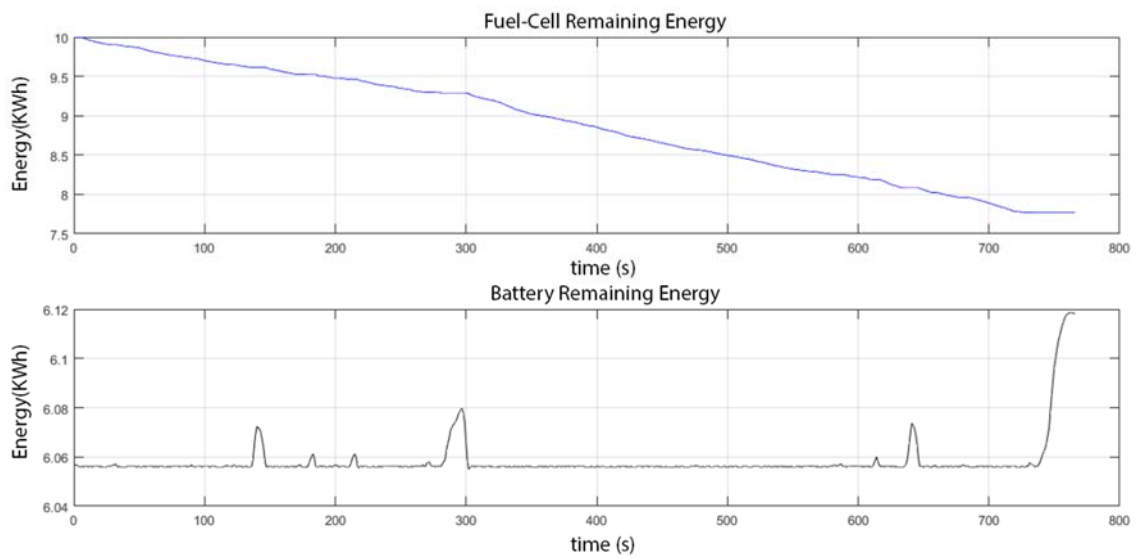


Figure 6.10(b) fuel cell and battery remaining energy in DP

Comparing these two energy management systems it becomes clear that each system has its own advantage over the other. The Dynamic programming approach shows a good energy deployment. While the rule base is depending more on the fuel cell rather than the battery. The dynamic programming on the other hand requires a quick startup and shut down of the fuel cell.

This could not be applicable till now since these times are around 30 seconds each. Future work on the fuel cell in the rule base system must be done to turn on and off the fuel cell. This should take into consideration the required time for the fuel cell startup and shutdown.

E. Results

Car1 having the specifications as described earlier was simulated at UDDS and HWFET under CS and CD modes. Also, the ambient temperature was varied between 25°C and 40°C . Furthermore, an inclination angle of 0.573° was added to the road, which means that a 10m in height is added for every 1km covered by the vehicle. The results are presented below in tables 6.7, 6.8, 6.9 and 6.10. A coding system is used in the below tables to represent the conditions under which each run was done. For example “CD-40-inc” stands for a battery under a charge depletion mode at 40°C with the mentioned inclination angle.

Table 6.8: FCHEV-20 Operation at UDSS

	CD-25-0	CD-40-0	CD-25-inc	CD-40-inc	CS-25-0	CS-40-0	CS-25-inc	CS-40-inc
Distance Travelled (km)				11.99				
Battery initial SOC (pu)		0.9					0.55	
FC initial Temperature (K)				353				
Battery initial Temperature (K)	308	313	308	313	308	313	308	313
Hydrogen consumed (g)	55.31	55.04	55.86	55.65	126.1	124.8	164	164.9
Battery Energy (kWh)	1.07	1.08	1.69	1.7	-0.18	-0.17	-0.16	-0.16
FC Energy (kWh)	1.14	1.14	1.15	1.15	2.39	2.37	3.05	3.08
Battery final SOC (pu)	0.7	0.7	0.61	0.61	0.55	0.55	0.55	0.55
FC Final Temperature (K)	333.6	340.2	333.7	340.3	340	340.6	343.6	348.3
Battery Final Temperature (K)	299.2	314.1	299.4	314.3	298.7	313.7	298.7	313.6

Table 6.9: FCHEV-20 Operation at HWFET

Table 6.10: FCHEV-40 Operation at UDSS

	CD-25-0	CD-40-0	CD-25-inc	CD-40-inc	CS-25-0	CS-40-0	CS-25-inc	CS-40-inc
Distance Travelled (km)	CD-25-0	CD-40-0	CD-25-inc	CD-40-inc	CS-25-0	CS-40-0	CS-25-inc	CS-40-inc
Distance Travelled (km)			0.9	11.99			0.55	
Battery initial SOC (pu)			0.9	353			0.55	
FC initial Temperature (K)				353				
Battery initial Temperature (K)	308	313	308	313	308	313	308	313
Battery initial Temperature (K)	308	313	308	313	308	313	308	313
Hydrogen consumed (g)	30.74	30.5	82.92	79.44	151.2	150.5	211.6	210.4
Hydrogen consumed (g)	46.68	46.45	46.08	46.45	-0.282	-0.1305	-0.747	-0.144
Battery Energy (kWh)	0.89	0.89	2.09	2.08	-0.278	-0.275	3.81	-9.89
Battery Energy (kWh)	0.96	0.96	0.96	0.96	0.93	0.93	0.95	0.93
Battery final SOC (pu)	0.96	0.96	0.96	0.96	0.93	0.93	0.95	0.93
Battery final Temperature (K)	330.8	339.9	397.9	397.6	342.5	349.5	348.5	392.5

Battery Final Temperature (K)	333.6	340.2	333.6	340.2	242.4	349.4	345.5	350.3
Battery Final Temperature (K)	300.6	315.3	300.4	315.1	298.9	313.8	298.7	313.6
Temperature (K)	307.4	313.6	307.6	313.6	308.8	313.8	308.7	313.7

Table 6.11: FCHEV-40 Operation at HWFET

	CD-25-0	CD-40-0	CD-25-inc	CD-40-inc	CS-25-0	CS-40-0	CS-25-inc	CS-40-inc
Distance Travelled (km)	16.51							
Battery initial SOC (pu)	0.9			0.55				
FC initial Temperature(K)	353							
Battery initial Temperature (K)	308	313	308	313	308	313	308	313
Hydrogen consumed (g)	26.1	25.99	26.1	25.99	160.2	158.8	227.7	224.5
Battery Energy (kWh)	2.11	2.11	3.15	3.15	-0.18	0.18	-0.15	-0.15
FC Energy (kWh)	0.53	0.53	0.53	0.53	2.88	2.88	3.98	3.94
Battery final SOC (pu)	0.76	0.76	0.69	0.69	0.55	0.55	0.55	0.55
FC Final Temperature(K)	331.2	337.3	331.2	337.7	346.4	352.9	351	351
Battery Final Temperature (K)	308.4	314	307.6	314.2	308.3	313.3	308.2	313.2

From the above results a trend can be noticed:

With the increase in the road inclination angle, the battery energy increases which causes the increase in the battery temperature while the Hydrogen consumption and FC energy remain unchanged. This is the case if the battery didn't reach the mid SOC. Once this is reached, the battery will enter a CS mode.

In this mode, the FC energy increases along with the hydrogen consumption and the fuel cell temperature. The battery on the other hand gets charged from excess energy coming from the fuel cell.

Car3: All-battery

The above car model can be operated as a pure electric car if the fuel cell is removed by setting its maximum current to zero. It is then tested as above under different ambient temperatures and different inclination angles.

Table 6.12: All- Battery Car Operation at UDDS

	CD-25-0	CD-40-0	CD-25-inc	CD-40-inc
Distance Travelled (km)	11.99			
Battery initial SOC (pu)	0.9			
Battery initial Temperature (K)	308	313	308	313
Battery Energy (kWh)	1.874	1.879	2.47	2.462
Battery final SOC (pu)	0.77	0.77	0.73	0.73
Battery Final Temperature (K)	298.6	313.7	298.6	313.6

Table 6.13: All- Battery Car Operation at HWFET

	CD-25-0	CD-40-0	CD-25-inc	CD-40inc
Distance Travelled (km)	16.51			
Battery initial SOC (pu)	0.9			
Battery initial Temperature (K)	308	313	308	313
Battery Energy (kWh)	2.314	2.316	3.193	3.193
Battery final SOC (pu)	0.75	0.75	0.69	0.69
Battery Final Temperature (K)	299	314	299.3	314.1

F. 40 mile vehicle detailed results

Results obtained for the FCHEV 40 in the UDDS driving cycle is shown below. These results include the FC and battery power demand obtained from the EMS. The energy remaining in the FC and the battery, the auxiliary power, the inlet and outlet cooling temperature, the heat rate and temperature variation in the fuel cell and the battery, and the hydrogen tank temperature and pressure.

1. CD-25-0

As discussed earlier, the EMS divides the power demand between the fuel cell and the battery. Figure 6.11 shows the power required during this operation, where the fuel cell supplies a constant value of value equals to its minimum rated power. The battery on the other hand, supplies the rest of the needed power and recharge during regenerative braking.

The fuel cell energy (Figure 6.12(a)) is decreasing linearly, this is because the power demand is constant all the time. The battery energy (Figure 6.12(b)) is decreasing when the power demand is positive (discharging) and increasing with negative power (charging). The battery has a negative slope over time, which shows that the battery is depleting its power.

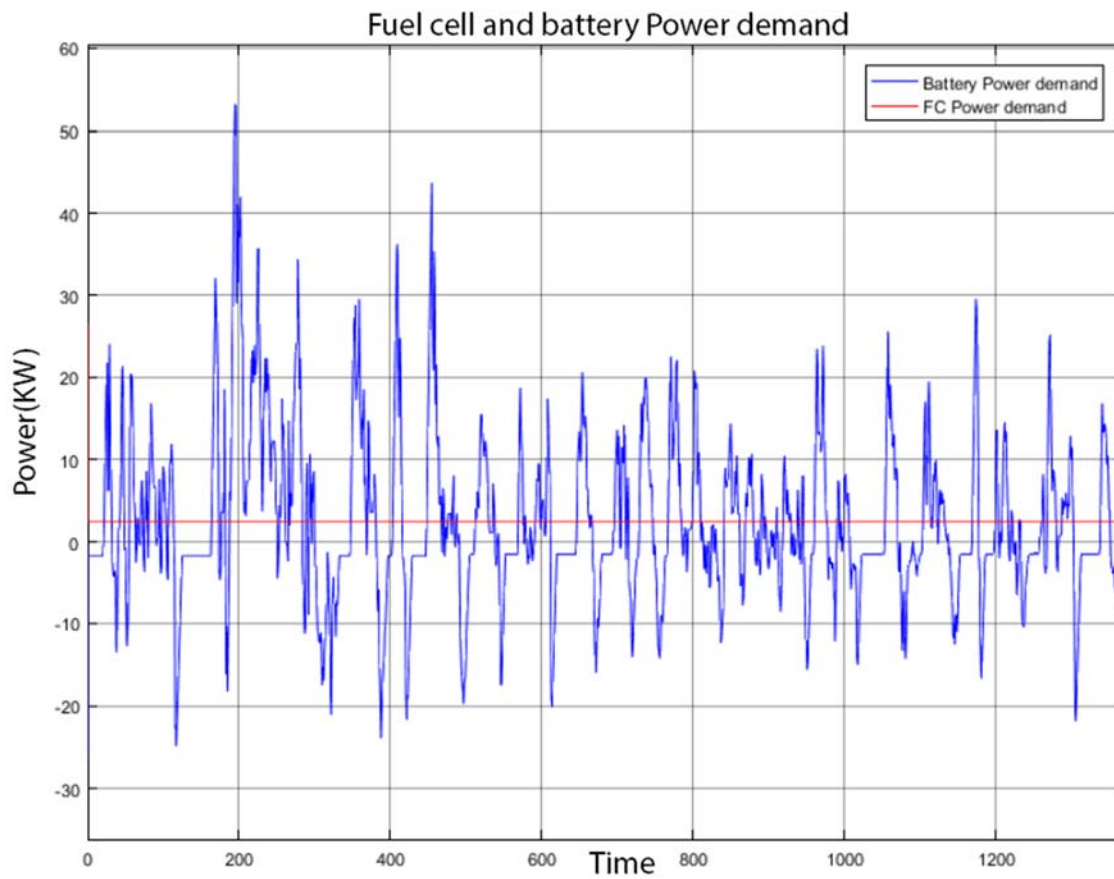


Figure 6.11: fuel cell and battery Power supplied

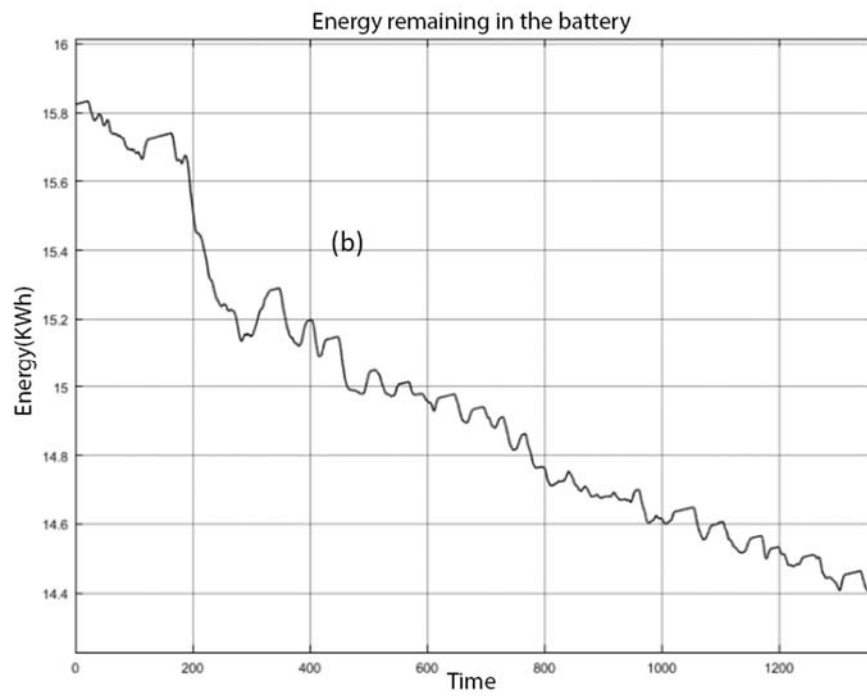
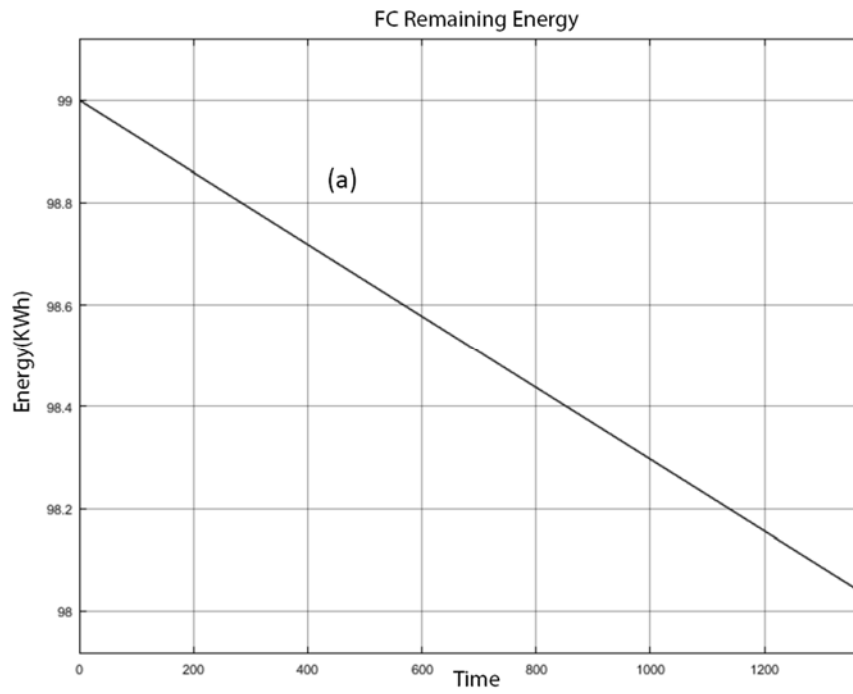


Figure 6.12: fuel cell (a) and battery (b) energy remaining

The auxiliary power shown in Figure 6.13 up until 430 seconds is constant and equal to the summation of the compressor power and the cooling pumps power. After that time, the battery cooling fan turns on and its corresponding power is added to the total auxiliary power.

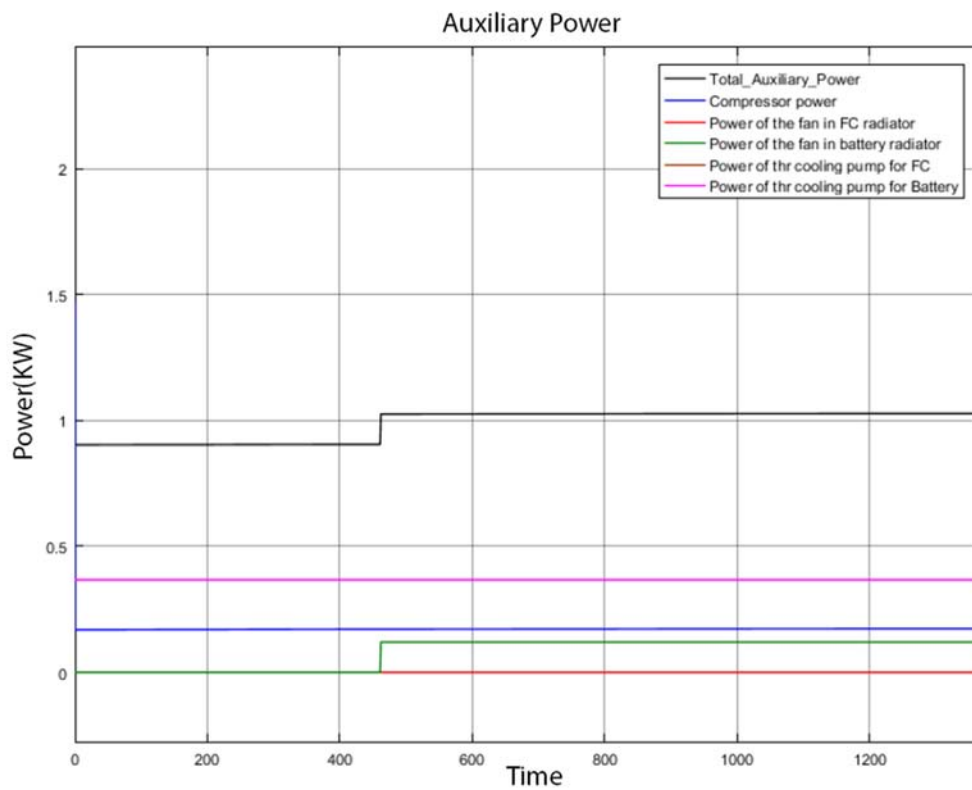


Figure 6.13: Auxiliary power

The heat rates in the fuel cell during the entire driving cycle are shown in Figure 6.14(a). The generated heat (Q_g) and the radiated heat (Q_r) have constant values, while the convected heat (Q_{con}) is varying with the car speed. On the other hand, the heat lost to the cooling system (Q_{cc}) is zero; this is because the heat lost to the environment via convection and radiation were sufficient to cool the fuel cell. We can see from Figure 6.15(a) that the fuel cell temperature is decreasing without the help of the cooling system.

For the battery (Figure 6.14(b)), the heat generated (Q_g) is not constant and is peaking at high power demands. The heat lost to the cooling system is zero up until 430 seconds, this is where the fan turns on to cool the liquid passing through the radiator that in turn will cool the battery pack. Figure 6.15(b) shows the increase in the battery temperature until 430 seconds, after that the fan turn on which increases the heat lost to the cooling system and hence decreases the battery temperature.

The hydrogen tank pressure and temperature variations are shown in Figures 6.16(a) and 6.16(b) respectively. It can be seen that with the hydrogen consumption, the tank pressure and temperature decrease in a linear manner.

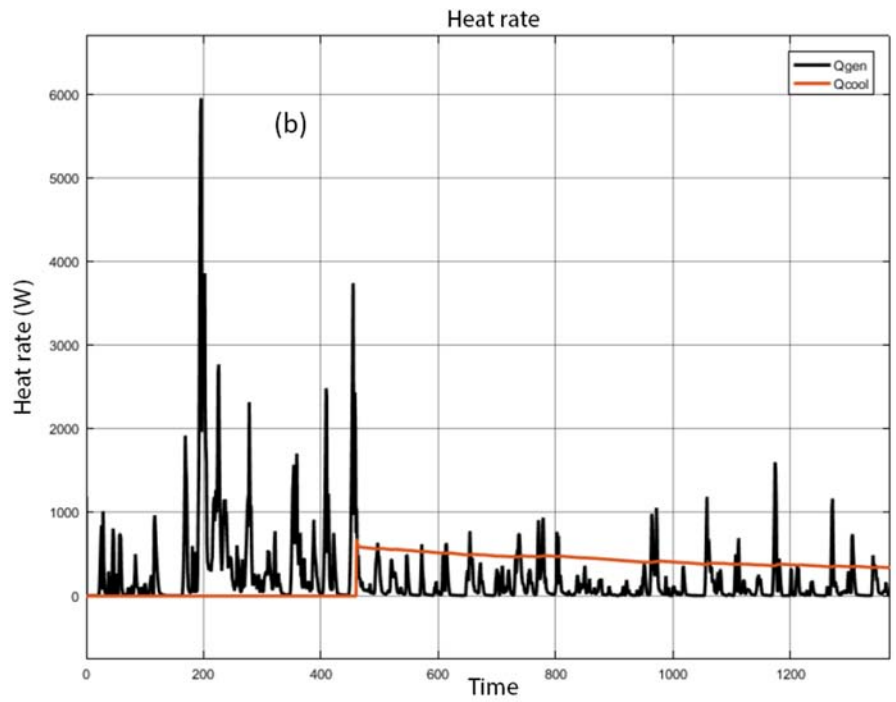
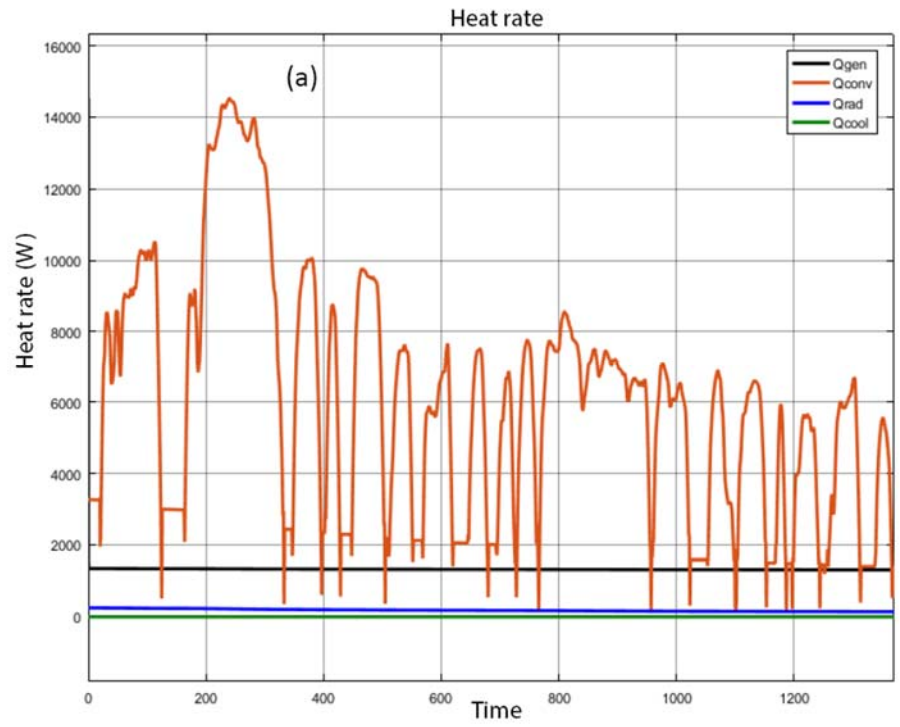


Figure 6.14: Heat rates in Fuel cell (a) and battery (b)

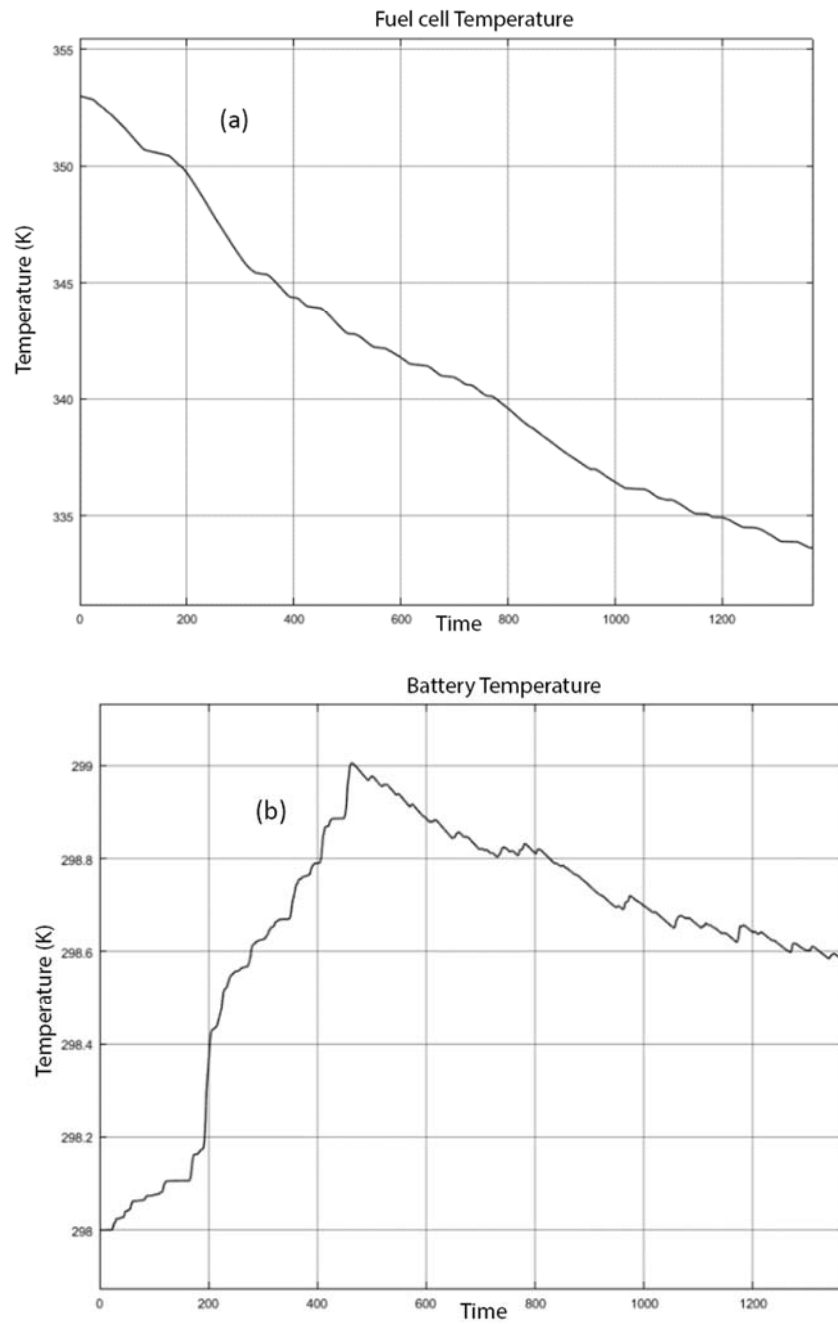


Figure 6.15: Fuel cell (a) and battery (b) Temperatures

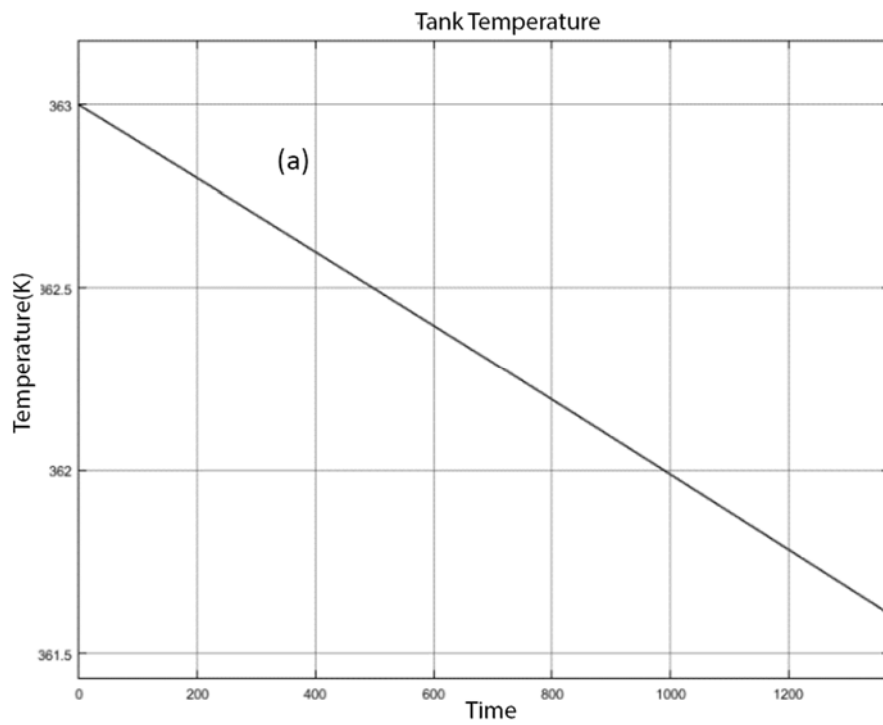
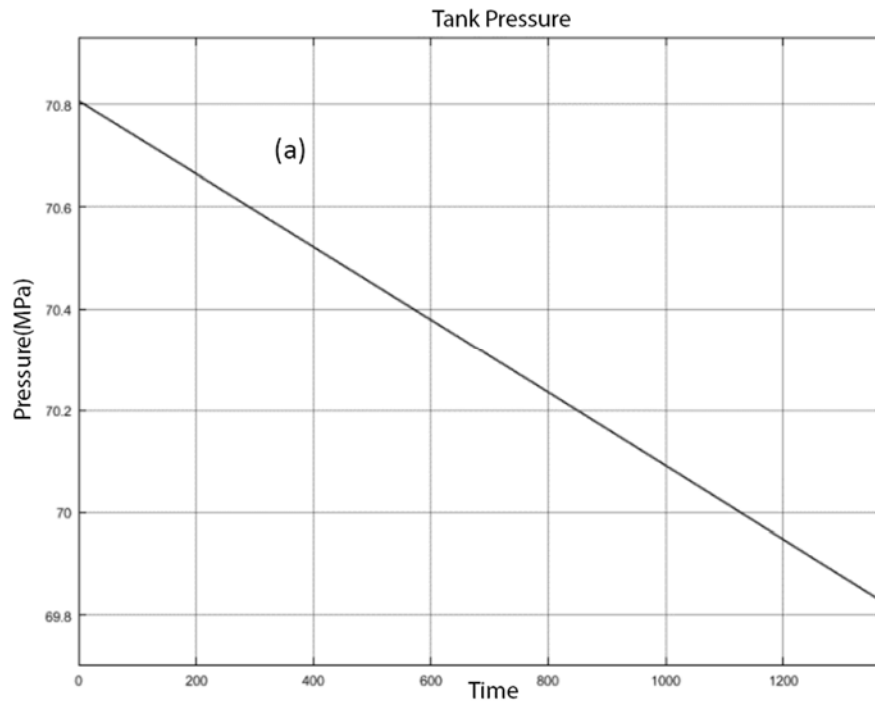


Figure 6.16: Pressure (a) and temperature (b) variation in hydrogen tank

2. *CS-25-0.01*

With the increase in the road inclination angle and when the battery is set to the CS mode, the following power demand is obtained in Figure 6.17. The fuel cell power demand is no longer at the minimum and the battery power decreased. This can also be seen in Figure 6.18(a) where the fuel cell remaining energy is decreasing but not so linearly as above. The battery energy in Figure 6.18(b) is decreasing when the power demand is positive (discharging) and increasing with negative power (charging). The battery energy has a positive slope over time, which shows an inability of the current rule-base EMS to keep the battery at a minimum specified level.

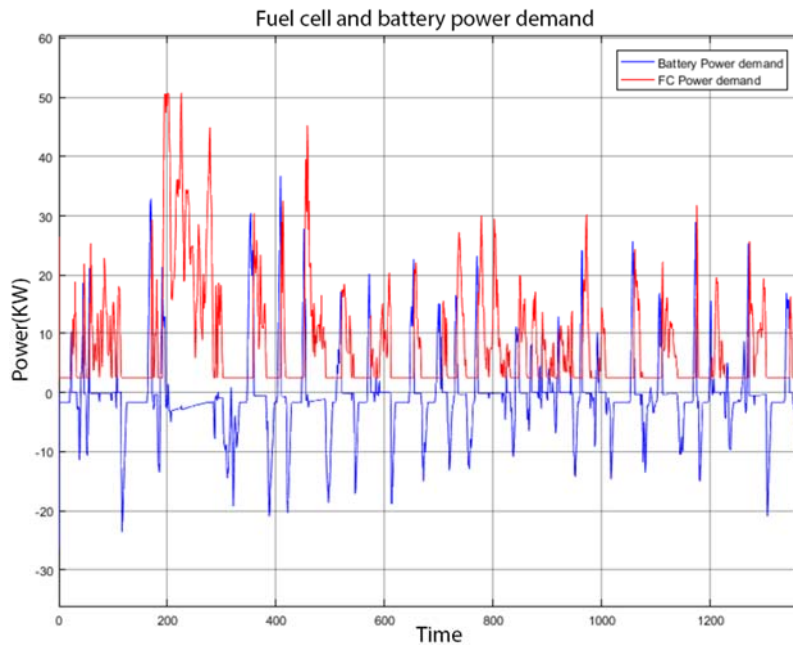


Figure 6.17: fuel cell and battery Power supplied

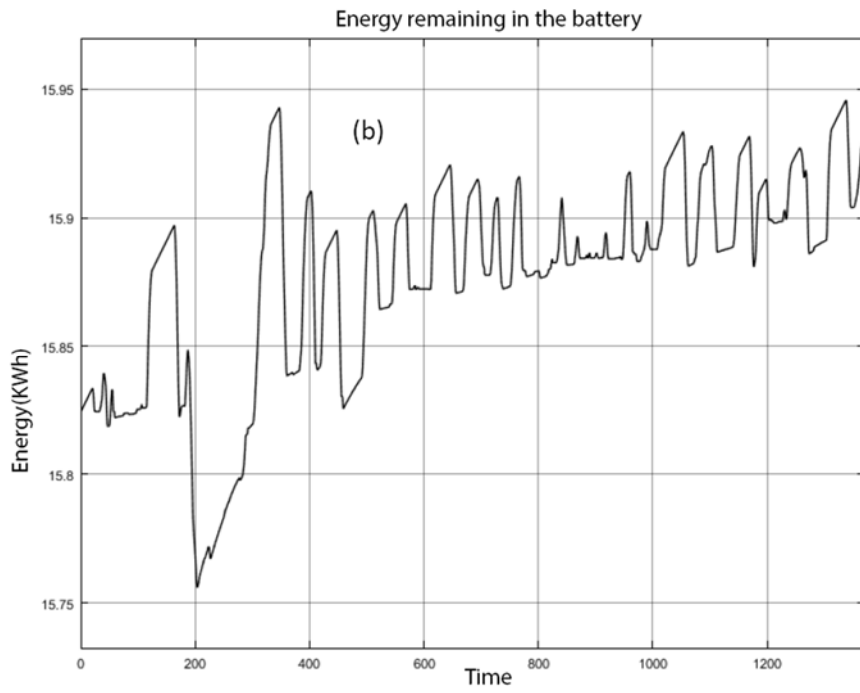
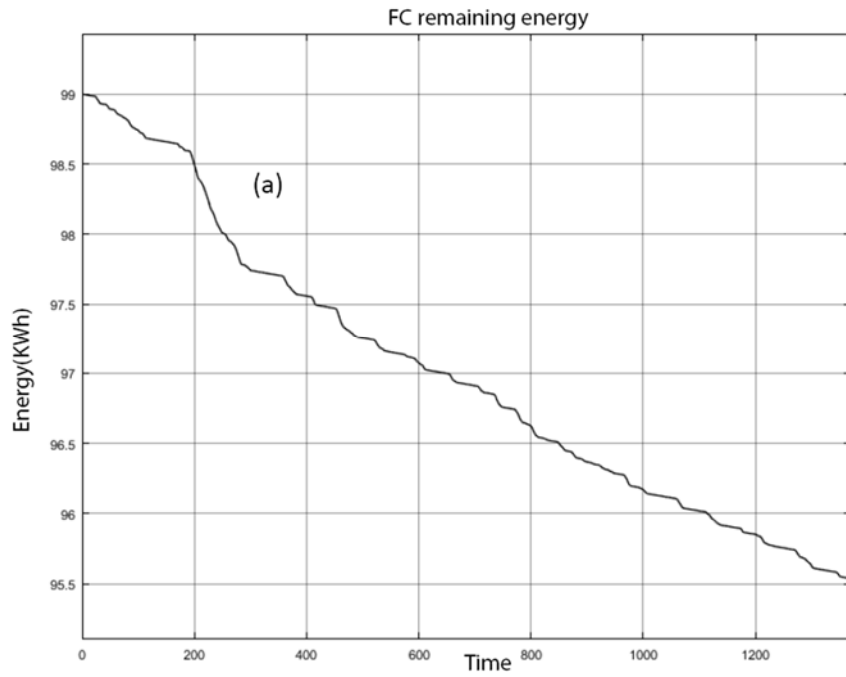


Figure 6.18: fuel cell (a) and battery (b) energy remaining

Now that the fuel cell power demand is no longer constant, the air flow rate requested by the fuel cell is also varying. This is why the compressor power is as shown in Figure 6.19. With higher power demand the fuel cell temperature increases (Figure 6.21(a)) hence the cooling fan responsible to cool the fuel cell radiator will turn on and then turn off again when the temperature drops below a certain value .

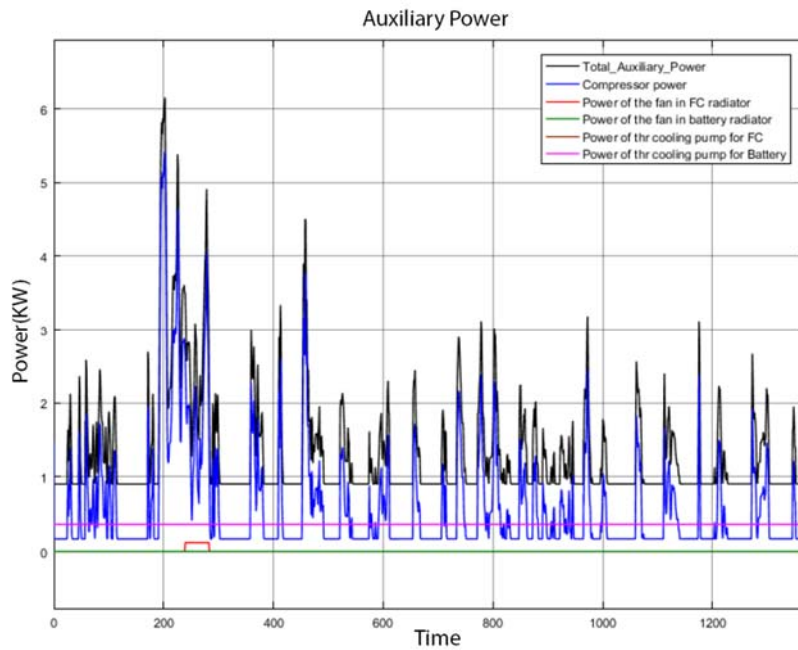
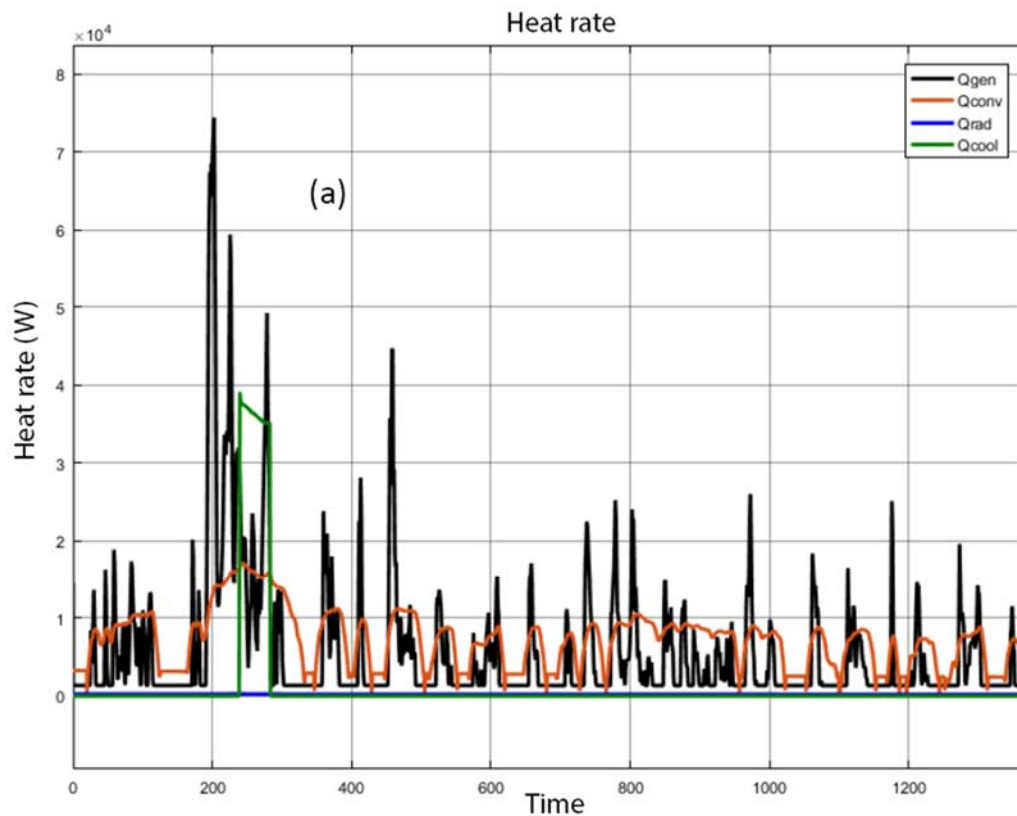


Figure 6.19: Auxiliary power

The heat rates in the fuel cell during the entire driving cycle are shown in Figure 6.20(a). The generated heat (Q_g) is no longer constant, and the heat convection (Q_{con}) is varying with the car speed. On the other hand, the heat lost to the cooling system (Q_{cc}) is zero except when the fan turns on (240 sec-280 sec); this is because the fuel cell temperature increased above the acceptable range (at 240 sec) which triggered the fan.

In the battery, the heat generated (Q_g) is not constant and is peaking at high power demands. The heat lost to the cooling system is zero; this is because the battery temperature did not exceed the acceptable range yet. Figure 6.20(b) shows the increase in the battery temperature over the entire cycle.

The hydrogen tank pressure and temperature variations are shown in Figures 6.22(a) and 6.22(b) respectively. It can be seen that with the hydrogen consumption, the tank pressure and temperature decrease but are no longer linear.



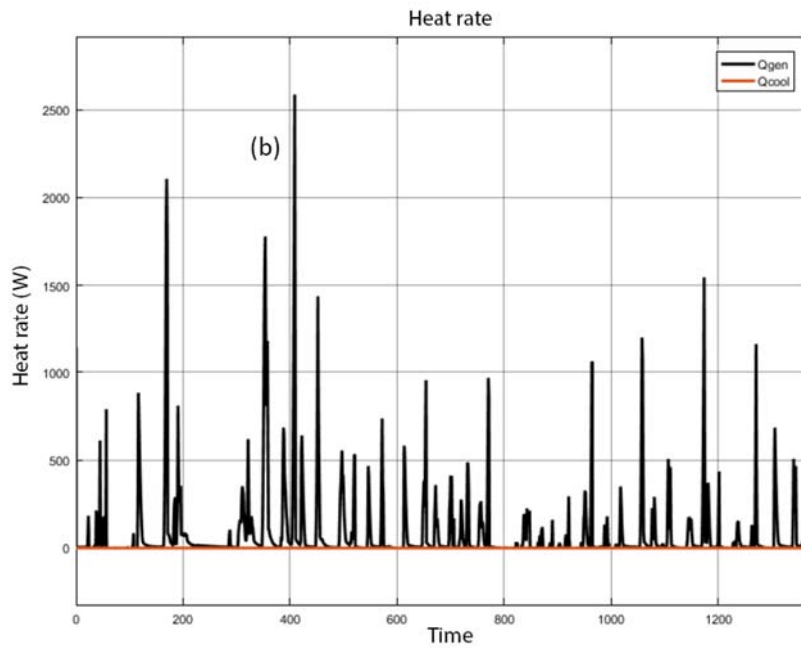
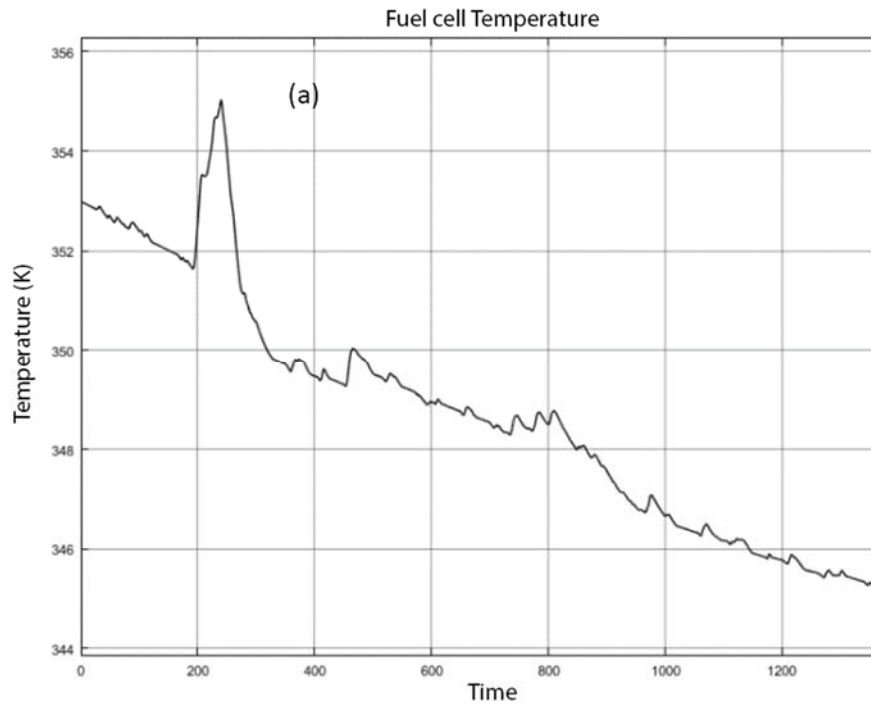


Figure 6.20: Heat rates in Fuel cell (a) and battery (b)



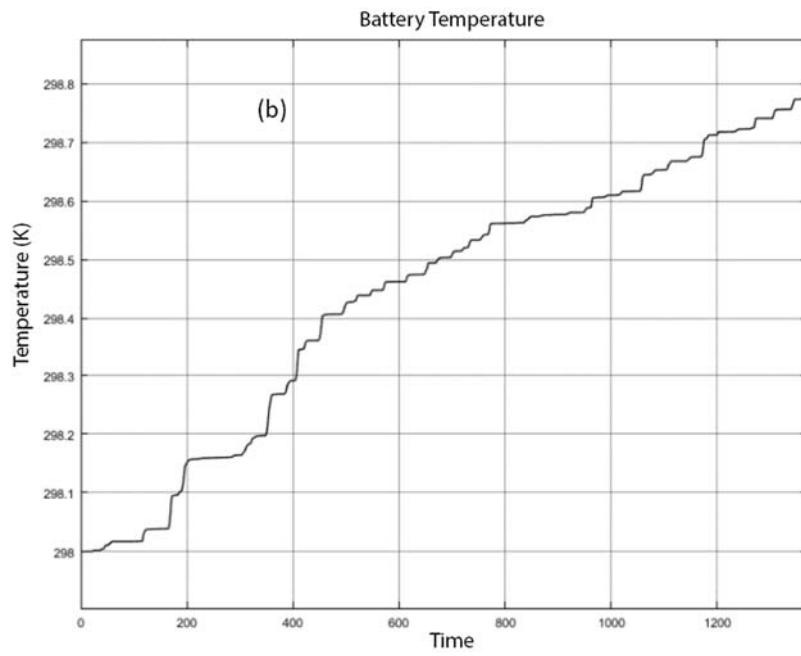


Figure 6.21: Fuel cell (a) and battery (b) Temperatures

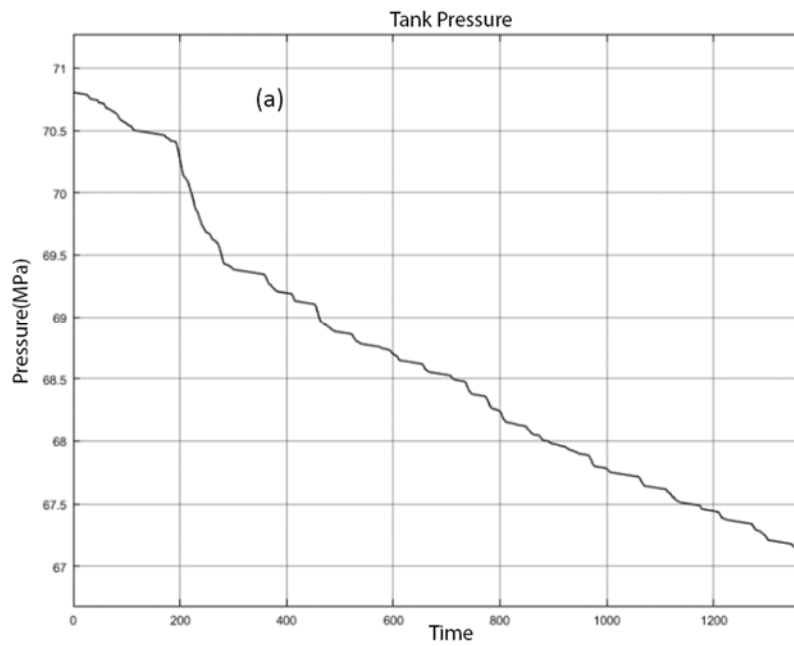
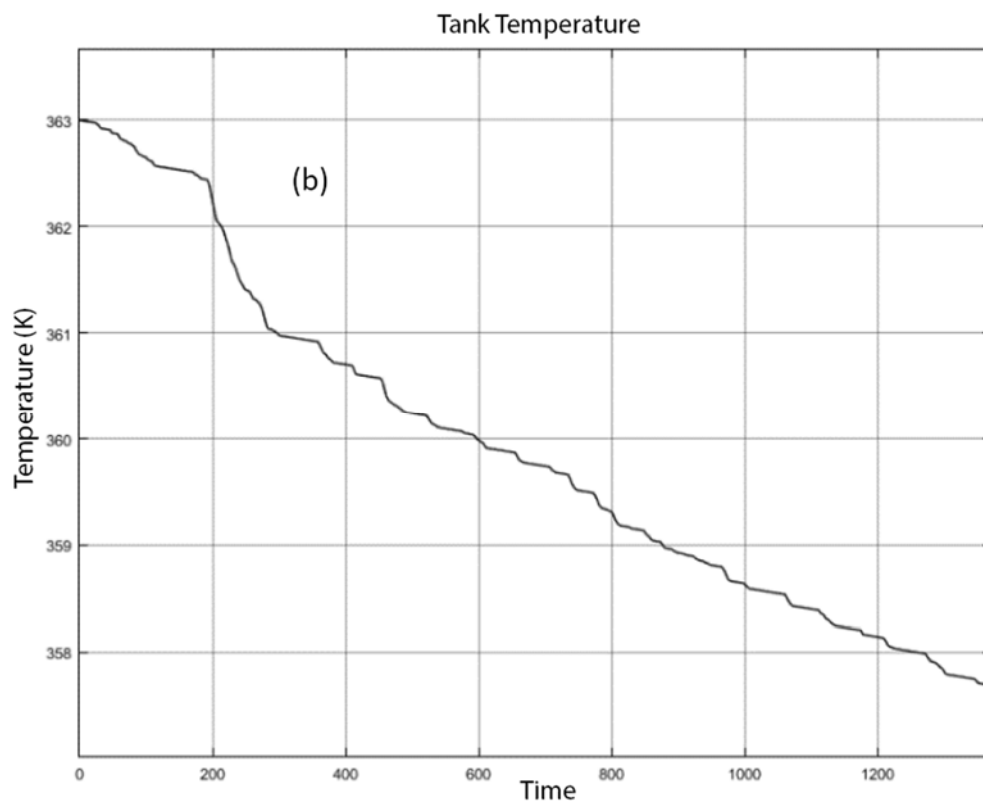


Figure 6.22: Pressure (a) and temperature (b) variation in hydrogen tank



CONCLUSION

Heat generation can affect the performance of the fuel cell or even damage its membrane. It is also known that temperature variations in the battery pack could affect its charging and discharging capabilities [30]. For these reasons, cooling systems were adopted to increase the efficiency of the mentioned elements. To do so, for the fuel cell as an example, an electrical model was developed and integrated to a thermal model that enabled the calculation of the FC temperature. The thermal model involves the modeling of the cooling system and the heat loss by convection and radiation. An algebraic representation was used to model the electrical behavior of the FC and the battery, and a dynamic equation based on the conservation of heat was used to determine the temperature variations. This model was developed in MATLAB - SIMULINK and tested under different power demand conditions. From these models we were able to calculate the cell temperature given the ambient temperature and the required power demand of the fuel cell. This simplified model was tested under different drive cycles with varying ambient conditions. A similar approach was followed to develop the electrical and thermal models of the Li-ion battery used. Same as in the fuel cell, the output voltage of the battery was modeled with temperature variations.

This research was concerned with the thermal effect on a FC vehicle, and designing an appropriate cooling system for its optimum operation. In this respect, the discussed models were put together with an energy management system of a fuel cell car based on the Rule base method. Finally the expanded car model was tested under several battery modes

(CS and CD) with different drive cycles and ambient temperatures.

The results show high heat and temperature variations inside the car. When the fuel cell is operating at minimum power, the natural air flowing inside the car was enough to cool the FC without the use of the cooling liquid. However, this is not the case when the FC is supplying higher power where the temperature starts to rise and hence the cooling system becomes necessary to cool down the FC. The battery in this design was enclosed so natural cooling was prevented and hence the heat dissipated only through the cooling system. From the above results, it is obvious that the cooling system is performing well and is cooling the two components once their temperatures rises above a certain value.

When operating at CD mode, the vehicle will be relying more on the battery to supply the energy demand of the vehicle keeping the fuel cell power at the minimum value. While in CS mode, the battery will supply the minimum power and the rest is supplied by the FC. The vehicle was also tested with an increased inclination angle and ambient temperatures. When the inclination angle was increased the total power demand in the vehicle also increased. While when increasing the ambient temperature, the FC and battery temperatures increased more which made the vehicle more relying on the cooling system.

Further work must be done on the EMS to allow the shutdown of the FC while taking into consideration the startup and shutdown periods.

REFERENCES

1. Chris Rayment, Scott Sherwin, Introduction to Fuel Cell Technology
2. Kay Damen, Martijn van Troost, André Faaij, Wim Turkenburg, "A comparison of electricity and hydrogen production systems with CO₂ capture and storage", journal of Progress in Energy and Combustion Science Vol.32, 2006, 215–246.
3. James Larminie, Andrew Dicks, "Fuel cell systems explained", second edition, J. Wiley 2003.
4. Syed Mushahid Hussain Hashmi (2010) ,"Konzepte zur Kühlung von PEM-Brennstoffzellen" (Cooling Strategies for PEM FC Stacks), Universität der Bundeswehr Hamburg, Master's dissertation,2010
5. Idoia San Martín, Alfredo Ursúa, Pablo Sanchis, Modelling of PEM Fuel Cell Performance: Steady-State and Dynamic Experimental Validation, journal of Open Access Energies, February 2014, pages: 670-700.
6. Setareh Shahsavari, Andrew Desouza, Majid Bahrami, Erik Kjeang, Thermal analysis of air-cooled PEM fuel cells, International journal of hydrogen energy Vol.37,2012, pages: 18261 – 18271.
7. J.D. Rojas, C. Ocampo Martinez, C.Kunusch, Thermal Modelling Approach and Model Predictive Control of a Water-cooled PEM Fuel Cell System.
8. Oliver Tremblay, Louis-A. Dessaint, and Abdel-illah Dekkiche, "A Generic Battery Model for the Dynamic Simulation of Hybrid Electric Vehicles", IEEE Vehicle Power and Propulsion Conference, 2007. Arlington, TX , 9-12 Sept. 2007, Pages:284 – 289
9. Hongwen He, Rui Xiong and Jinxin Fan, Evaluation of Lithium-Ion Battery Equivalent Circuit Models for State of Charge Estimation by an Experimental Approach, journal of Open Access Energies, 29 March 2011.
10. Joya Zeitouny, Jihad Bou Merhi, Jana Chalak, Sami Karaki, Estimation of Battery Internal Parameters.2015 IEEE International Conference on Industrial Technology (ICIT), Seville, Spain, March 17, 2015.
11. Feng Leng, Cher Ming Tan, Michael Pecht, Effect of temperature on the aging rate of Li Ion battery operating above room temperature, journal of scientific reports, August 2015.
12. Ahmad Pesaran, Ph.D. Shriram Santhanagopalan, Gi-Heon Kim, Addressing the Impact of Temperature Extremes on Large Format Li-Ion Batteries for Vehicle Applications, 30TH INTERNATIONAL BATTERY SEMINAR Ft. Lauderdale, Florida March November 2013
13. Ahmad PESARAN, Cooling and Preheating of Batteries in Hybrid Electric Vehicles, The 6th ASME-JSME Thermal Engineering Joint Conference, March 2003.
14. Giorgio Rizzoni, Lino Guzzella, and Bernd M. Baumann, Unified Modeling of Hybrid Electric Vehicle Drivetrains. IEEE/ASME transactions on mechatronics, vol. 4, no. 3, September 1999

15. J. Bernard, S.Delprat, T.M.Guerra, F.N.Buchi, Fuel efficient power management strategy for fuel cell hybrid powertrains, *Journal of Control Engineering Practice* Vol.18, pages: 408–417, 2010
 16. Sami H. Karaki, Rabih Jabr, Riad Chedid, and Ferdinand Panik, Optimal Energy Management of Hybrid Fuel Cell Electric Vehicles, SAE 2015-01-1359.
 17. Sami H. Karaki, Rafika Dinnawi, Rabih Jabr, Riad Chedid, and Ferdinand Panik, Fuel Cell Hybrid Electric Vehicle Sizing using Ordinal Optimization, 2015-01-0155.
 18. Carla Majed, Sami H. Karaki, Rabih Jabr, and Ferdinand Panik, Near Optimal Control of Fuel Cell Hybrid Electric Vehicles in Real-Time. SAE World Congress 2016, Technical Paper # 2016-01-1390.
 19. Han-Sang Kim, Kyoungdoug Min, Experimental investigation of dynamic responses of a transparent PEM fuel cell to step changes in cell current density with operating temperature, *Journal of Mechanical Science and Technology*, July 3 2008.
 20. Ashley Fly, Thermal and water management of evaporative cooled fuel cell vehicles, Doctoral thesis
 21. M.G.Santarelli, M.F.Torchio, P.Cochis, "Parameters estimation of a PEM fuel cell polarization curve and analysis of their behaviour with temperature", *Journal of Power Sources*, vol. 159, pp. 824-835, 2006.
 22. Deborah A.Kaminiski, Michael K.Jensin, Introduction to thermal and fluids engineering.
 23. Z. Belkhiri, M. Zeroual, H. Ben Moussa ,B. Zitouni, Effect of temperature and water content on the performance of PEM fuel cell, *Revue des Energies Renouvelables* Vol. 14 N°1 (2011) 121 – 130
 24. MIT Electric Vehicle Team, A Guide to Understanding Battery Specifications, December 2008
 25. Long Lam, A Practical Circuit based Model for State of Health Estimation of Li ion Battery Cells in Electric Vehicles August 2011.
 26. Mengbo Ji, Zidong Wei, A Review of Water Management in Polymer Electrolyte Membrane Fuel Cells, *Energies* 2009, 2, 1057-1106
 27. Matthew Carl, Dana Guy, Brett Leyendecker, Austin Miller, and Xuejun Fan, THE THEORETICAL AND EXPERIMENTAL INVESTIGATION OF THE HEAT TRANSFER PROCESS OF AN AUTOMOBILE RADIATOR
 28. Ho-Seong Lee , Choong-Won Cho , Jae-Hyeong Seo , Moo-Yeon Lee, Cooling Performance Characteristics of the Stack Thermal Management System for Fuel Cell Electric Vehicles under Actual Driving Conditions.
 29. Andrew Burnham, Updated Vehicle Specifications in the GREET Vehicle-Cycle Model, Center for Transportation Research, Argonne National Laboratory, July 2012
- Ahmad PESARAN, Cooling and Preheating of Batteries in Hybrid Electric Vehicles, The 6th ASME-JSME Thermal Engineering Joint Conference, March 2003.

